

MOLECULAR CLOUD EVOLUTION II. FROM CLOUD FORMATION TO THE EARLY STAGES OF STAR FORMATION IN DECAYING CONDITIONS

ENRIQUE VÁZQUEZ-SEMADENI¹, GILBERTO C. GÓMEZ¹, A. KATHARINA JAPPSSEN^{2,3}, JAVIER BALLESTEROS-PAREDES¹, RICARDO F. GONZÁLEZ¹ AND RALF S. KLESSEN⁴

Submitted to The Astrophysical Journal

ABSTRACT

We study the formation of giant dense cloud complexes and of stars within them by means of SPH numerical simulations of the collision of gas streams (“inflows”) in the warm neutral medium (WNM) at moderately supersonic velocities. The collisions cause compression, cooling and turbulence generation in the gas, forming a cloud that then becomes self-gravitating and begins to collapse globally. Simultaneously, the turbulent, nonlinear density fluctuations induce fast, local collapse events. The simulations show that: a) The clouds are *not* in a state of equilibrium. Instead, they undergo secular evolution. During the early stages of the evolution, their mass and gravitational energy E_g increase steadily, while the turbulent energy E_k reaches a plateau. b) When E_g becomes comparable to E_k , global collapse begins, causing a simultaneous increase in $|E_g|$ and E_k that maintains a near-equipartition condition $|E_g| \sim 2E_k$. c) Longer inflow durations delay the onset of global and local collapse, by maintaining a higher turbulent velocity dispersion in the cloud over longer times. d) The star formation rate is large from the beginning, without any period of slow and accelerating star formation. e) The column densities of the local star-forming clumps are very similar to reported values of the column density required for molecule formation, suggesting that locally molecular gas and star formation occur nearly simultaneously. The MC formation mechanism discussed here naturally explains the apparent “virialized” state of MCs and the ubiquitous presence of HI halos around them. Also, within their assumptions, our simulations support the scenario of rapid star formation *after* MCs are formed, although long ($\gtrsim 15$ Myr) accumulation periods do occur during which the clouds build up their gravitational energy, and which are expected to be spent in the atomic phase.

Subject headings: Instabilities — ISM: clouds — ISM: evolution — Shock waves — Stars: formation— Turbulence

1. INTRODUCTION

The evolution of molecular clouds (MCs) remains an unsolved problem to date. While traditionally MCs have been thought of as virialized structures in the interstellar medium (ISM) (e.g., de Jong, Boland & Dalgarno 1980; McKee et al. 1993; Blitz & Williams 1999; McKee 1999), with relatively long lifetimes (Blitz & Shu 1980) and a significant delay before they begin forming stars (e.g. Palla & Stahler 2000, 2002; Tassis & Mouschovias 2004; Mouschovias, Tassis & Kunz 2006), recent studies have suggested that MCs begin forming stars shortly after they themselves form, and are non-equilibrium entities (Ballesteros-Paredes, Vázquez-Semadeni & Scalo 1999; Ballesteros-Paredes, Hartmann & Vázquez-Semadeni 1999; Elmegreen 2000; Hartmann, Ballesteros-Paredes & Bergin 2001; Vázquez-Semadeni, Ballesteros-Paredes & Klessen

2003; Vázquez-Semadeni et al. 2006; Ballesteros-Paredes & Hartmann 2006; Ballesteros-Paredes 2006, see also the reviews by Mac Low & Klessen 2004 and Ballesteros-Paredes et al. 2006). One approach that can shed light on this problem is to perform numerical simulations of the MC formation process by generic compressions in the warm neutral medium (WNM). Numerous studies of this kind exist, although self-gravity has in general not been included (Hennebelle & Pérault 1999, 2000; Koyama & Inutsuka 2000, 2002; Inutsuka & Koyama 2004; Audit & Hennebelle 2005; Heitsch et al. 2005, 2006; Vázquez-Semadeni et al. 2006, hereafter Paper I).

These studies have shown that a substantial fraction of the internal turbulence, with velocity dispersions of up to a few km s^{-1} , can be produced in shock-bounded layers by a combined dynamical+thermal instability, whose nature is still not well determined (Hunter et al. 1986; Walder & Folini 1998, 2000; Koyama & Inutsuka 2002; Inutsuka & Koyama 2004; Heitsch et al. 2005, 2006; Folini & Walder 2006). Paper I also showed that the dense gas, there defined as the gas with densities larger than 100 cm^{-3} , is at systematically higher thermal pressures than the mean interstellar value by factors of 1.5–5, implying that MC formation by colliding streams of diffuse gas can account at least partially for the clouds’ excess pressure and turbulent nature.

Only a few works have included self-gravity in sim-

Electronic address: e.vazquez, g.gomez, j.ballesteros, rf.gonzalez@astro.uni-heidelberg.de

¹ Centro de Radioastronomía y Astrofísica (CRyA), Universidad Nacional Autónoma de México, Apdo. Postal 72-3 (Xangari), Morelia, Michoacán 58089, México

² Astrophysikalisches Institut Potsdam, An der Sternwarte 16, 14482 Potsdam, Germany

³ Canadian Institute for Theoretical Astrophysics (CITA), McLennan Physics Labs, 60 St. George Street, University of Toronto, Toronto, ON M5S 3H860, Canada

⁴ Institut für Theoretische Astrophysik / Zentrum für Astronomie der Universität Heidelberg, Albert-Überle-Str. 2, 69120 Heidelberg, Germany

ulations of colliding flows. The pioneering work of Hunter et al. (1986) considered the collision of supersonic streams within MCs, finding that the fragments produced by the dynamical instability (which they termed “Rayleigh-Taylor-like”) were able to accrete mass until they became gravitationally unstable and collapse. However, this study was designed to investigate flows *within* MCs rather than the formation of the clouds themselves, and so it considered much smaller (sub-parsec) scales and different density, temperature and cooling regimes than are relevant for the process of MC formation.

More recent numerical studies of MC formation not including self-gravity (Koyama & Inutsuka 2002; Heitsch et al. 2005) have estimated that the individual clumps formed in the compressed layer formed by the colliding streams are themselves gravitationally stable, although the entire compressed-gas complex would be gravitationally unstable, had self-gravity been included.

This raises the issue of whether the clumps can be considered in isolation. The question of which gas parcels are involved in the collapse of a particular object is a delicate one, and lies, for example, at the heart of the debate of whether competitive accretion is relevant or not in the process of star formation within molecular clouds: A model in which clumps are isolated dense objects immersed in a more tenuous, unbound medium leads to the conclusion that competitive accretion is irrelevant (Krumholz, McKee & Klein 2005). Instead, competitive accretion plays a central role (Bonnell et al. 1997; Klessen, Bate & Burkert 1998; Bonnell et al. 2001; Klessen & Burkert 2000, 2001; Klessen 2001a,b; Bonnell & Bate 2006) in a scenario in which the local density peaks are the “tips of the iceberg” of the density distribution, the flows are organized on much larger scales (Ballesteros-Paredes, Vázquez-Semadeni & Scalo 1999; Ballesteros-Paredes, Hartmann & Vázquez-Semadeni 1999; Bate, Bonnell & Bromm 2003), and the evolution and energetics of the density peaks cannot be considered in isolation, but as part of the global flow instead (Ballesteros-Paredes, Vázquez-Semadeni & Scalo 1999; Klessen, Heitsch & Mac Low 2000; Heitsch, Mac Low & Klessen 2001; Shadmehri, Vázquez-Semadeni & Ballesteros-Paredes 2002; Tilley & Pudritz 2004, 2005; Ballesteros-Paredes 2006; Dib et al 2006). In a similar fashion, then, accurate determination of whether gravitational collapse can be triggered by moderate-Mach number stream collisions in the WNM, requires to self-consistently include self-gravity in the numerical simulations.

Simulations of molecular cloud formation by the passage of a self-gravitating, clumpy medium through Galactic spiral shocks (Bonnell et al. 2006; Dobbs, Bonnell & Pringle 2006) have shown that realistic velocity dispersions and densities can be generated in the resulting post-shock clouds, which are furthermore driven to produce local collapse events leading to star formation, although a large fraction of the mass in the clouds remains gravitationally unbound. However, because these simulations were isothermal, the gas had to be assumed to already be clumpy and at very low temperatures (~ 100 K) *previous* to the passage through the shock, while recent studies including

cooling leading to thermal bistability of the atomic gas (Koyama & Inutsuka 2002; Audit & Hennebelle 2005; Heitsch et al. 2005, 2006, Paper I) suggest that the clumpiness is generated by the shock compression, which nonlinearly triggers the thermal instability, induces supersonic turbulence, and causes the formation of dense clumps in the compressed layers.

It is thus essential to model the evolution of the cloud within the frame of its more diffuse environment including both self-gravity and cooling. Not only this is indispensable in order to model the generation of turbulence and clumpiness, but also to model the cloud’s evolution as it exchanges mass and energy with its surroundings. Note that the generation of turbulence by the compression itself implies that the turbulence within the cloud is driven while the large-scale converging motions persist, and decaying afterwards. This is a mixed regime that also requires self-consistent modeling of the cloud and its surroundings, rather than, for example, random Fourier driving in closed boxes.

Finally, such a unified (or “holistic”) description of molecular cloud formation and evolution, as outlined by Vázquez-Semadeni, Ballesteros-Paredes & Klessen (2003), including the star formation epoch, allows also the investigation of a number of key problems, such as the evolutionary and star-formation timescales, the evolution of the cloud’s gravitational and kinetic energies, and whether it settles into virial equilibrium or not, and the effect of self-gravity on the cloud’s physical conditions.

In this paper we investigate numerically the evolution of interstellar gas as it collects from the WNM, shocks, suffers a phase transition to a cold and dense state, and finally begins to form stars, by means of numerical simulations of colliding gas streams in the WNM, in the presence of self-gravity and cooling leading to thermal instability. Since this is a problem that naturally collects large amounts of gas in small volumes, first by compression-triggered thermal instability and then by gravitational instability, it is convenient to use some Lagrangian numerical scheme, and we opt for a smoothed particle hydrodynamics code, sacrificing the possibility of including magnetic fields. We also omit for now a self-consistent description of the stellar feedback on the gas and of the chemistry. Thus, our simulations will not adequately describe the latest stages of MC evolution (in which stellar energy feedback may significantly influence the dynamics of the cloud) nor are they capable of predicting the transition from atomic to molecular gas accurately. We defer these tasks to subsequent papers.

The plan of the paper is as follows. In §2 we first give a qualitative description of the physical system, the main phenomena involved, and our expectations for the evolution. In §3 we describe the numerical code, the physical physical setting, and the choice of parameters. Then, in §4 we describe the results concerning the evolution of the cloud’s mass and its kinetic and gravitational energies, and the onset of star formation. In §5 we discuss the implications and limitations of the recent work. Finally, in §6 we present a summary and draw some conclusions.

2. QUALITATIVE DISCUSSION

It is convenient to first present an overview of the system, its expected evolution, and the physical processes

on which it relies (see also the description in Paper I). Since we are interested in studying the formation of a dense cloud out of the diffuse medium, we take as initial condition a uniform-density region within the WNM, of a few hundred parsecs across, with an initially compressive velocity field consisting of two oppositely-directed inflows with speed v_{inf} and Mach number \mathcal{M}_{inf} , with respect to the WNM temperature. This compressive field is generically representative of either the general turbulence in the WNM, or of motions triggered by some large scale agent, such as gravitational or Parker instabilities, or shell collisions. Since the velocity dispersion in the WNM is transonic (Kulkarni & Heiles 1987; Heiles & Troland 2003), we consider values of $\mathcal{M}_{\text{inf}} \sim 1$.

As is well known, the atomic ISM is thermally bistable, with two stable phases being able to coexist at the same pressure but different densities and temperatures, mediated by a thermally unstable range (Field 1965; Field, Goldsmith & Habing 1969). The collision of transonic WNM streams produces a thick shock-bounded slab, in which the gas is out of thermal equilibrium between radiative heating and cooling. This shocked slab is nonlinearly thermally unstable (Koyama & Inutsuka 2000; Kritsuk & Norman 2002), and as it flows towards the collision plane, it undergoes a phase transition to the cold neutral medium (CNM), causing the formation of a thin cold layer, (Hennebelle & Pérault 1999, 2000; Koyama & Inutsuka 2000, 2002; Inutsuka & Koyama 2004; Audit & Hennebelle 2005; Heitsch et al. 2005, 2006, Paper I). Subsequently, the boundary of this layer is destabilized, probably by a combination of thermal instability and nonlinear thin-shell instability (Vishniac 1994), producing fully-developed turbulence in the layer for sufficiently large \mathcal{M}_{inf} (Hunter et al. 1986; Koyama & Inutsuka 2002; Inutsuka & Koyama 2004; Heitsch et al. 2005, 2006, Paper I). As the layer becomes turbulent, it thickens, and becomes a fully three-dimensional structure (Paper I), to which we simply refer as “the cloud”.

Moreover, the thermal pressure in the dense cloud is in pressure balance with the total (thermal + ram) pressure in the inflows, which is significantly larger than the mean thermal pressure in the ISM (Paper I). Consequently, the density in the cold layer can reach densities significantly larger than those typical of the CNM. Thus, this cloud is turbulent, dense, and overpressured with respect to the mean ISM pressure; i.e., it has properties typical of molecular clouds (Paper I). The main missing link in this scenario is whether the atomic gas can be readily converted to molecular, although several studies suggest it is feasible (Bergin et al. 2004; Glover & Mac Low 2006). Since we do not incorporate any chemistry nor radiative transfer in our code, we cannot follow this transition self-consistently, and simply assume that once the *dense* gas has a sufficiently large column density (see below), it is rapidly converted to the molecular phase.

In summary, the compression produces a turbulent cloud of dense and cold gas. As it becomes denser and colder, its Jeans mass decreases substantially. Moreover, its own mass is increasing, so it rapidly becomes much more massive than its own Jeans mass. Also, as the cloud becomes more massive, its total gravitational energy (in absolute value) $|E_{\text{g}}|$ increases substantially, and eventu-

ally overcomes even its turbulent kinetic energy, and the cloud begins collapsing as a whole. Because it contains many Jeans masses, local collapse events begin to occur at the nonlinear density peaks produced by the turbulence, if gravity locally overcomes all available forms of support. Because the density enhancements are nonlinear, the local collapse events occur on shorter timescales than the global contraction.

The magnetic field should also be considered. Hennebelle & Pérault (2000) have shown that the transition from diffuse to dense gas can occur even in the presence of magnetic fields aligned with or oblique to the direction of compression. Moreover, most evidence, both theoretical and observational, points towards MCs and giant molecular complexes being magnetically supercritical or marginally critical at least (Crutcher 1999; Hartmann, Ballesteros-Paredes & Bergin 2001; Bourke et al. 2001; Crutcher, Heiles & Troland 2003). Since the magnetically supercritical case is not qualitatively different from the non-magnetic case, the above discussion is applicable to supercritical clouds as well.

Hartmann, Ballesteros-Paredes & Bergin (2001) have approximately quantified the above scenario, estimating that the accumulation time from the WNM should be of the order of 10–20 Myr, the accumulated gas must come from distances up to a few hundred parsecs, and that at the end of the accumulation period, the gas should be becoming molecular and self-gravitating at roughly the same time, because the column density for self-shielding and formation of molecular gas,

$$N_{\text{ss}} \sim 1 - 2 \times 10^{21} \text{ cm}^{-2}, \quad (1)$$

is very similar to that required for rendering the dense gas gravitationally unstable,

$$N_{\text{gi}} \sim 1.5 \times 10^{21} P_4^{1/2} \text{ cm}^{-2}, \quad (2)$$

where P_4 is the pressure expressed in units of 10^4 K cm^{-3} (see also Franco & Cox 1986). That is, the gas is converted to the molecular phase roughly simultaneously with the onset of gravitational instability, explaining why non-star-forming MCs are rare, at least in the solar neighborhood (Hartmann, Ballesteros-Paredes & Bergin 2001; Hartmann 2003; Ballesteros-Paredes & Hartmann 2006). Note, however, that this near equality is a coincidence (e.g., Elmegreen 1985, 1993a), since N_{gi} depends on the ambient pressure, and therefore non-star-forming molecular clouds may be more common in higher-pressure environments, possibly explaining observations that up to 30% of the GMCs appear to be starless in some external galaxies (Blitz et al. 2006). On the other hand, this result may be due in part to incompleteness effects. Indeed, recent Spitzer observations have uncovered young stellar objects in Galactic molecular cores previously believed to be starless (e.g., Craspi et al. 2005; Rho et al. 2006).

In the remainder of the paper, we proceed to quantify this scenario by means of numerical simulations designed for this purpose.

3. THE MODEL

3.1. Parameters and numerical scheme

We consider a cubic box of length L_{box} on a side, initially filled with WNM at a uniform density of $n_0 = 1 \text{ cm}^{-3}$, with a mean molecular weight of 1.27, so that the mean mass density is $\rho_0 = 2.12 \times 10^{-24} \text{ g cm}^{-3}$, which implies total masses of $6.58 \times 10^4 M_\odot$ and $5.26 \times 10^5 M_\odot$ for the two box sizes used, $L_{\text{box}} = 128 \text{ pc}$ and 256 pc , respectively. The gas has a temperature $T_0 = 5000 \text{ K}$, the thermal-equilibrium temperature at that density (cf. §3.3). Within the box, we set up two cylindrical and oppositely-directed inflows, each of length ℓ_{inf} , radius $r_{\text{inf}} = 32 \text{ pc}$, and speed $v_{\text{inf}} = \pm 9.20 \text{ km s}^{-1}$, corresponding to a Mach number $\mathcal{M}_{\text{inf}} = 1.22$ with respect to the sound speed of the undisturbed WNM, $c_{\text{WNM}} = 7.536 \text{ km s}^{-1}$ (see fig. 1). For the two values of ℓ_{inf} we consider here (48 pc and 112 pc), the masses of the cylindrical inflows are $1.13 \times 10^4 M_\odot$ and $2.64 \times 10^4 M_\odot$, respectively. To trigger the dynamical instability of the compressed slab, a fluctuating velocity field (computed in Fourier space) is initially imposed throughout the box at wavenumbers $4 \leq kL_{\text{box}} \leq 8$, and having amplitude $v_{\text{rms},i}$. The streams are directed along the x direction and collide at half the x extension of the box. Table 1 gives the values of these parameters for the simulations presented here. The runs are named mnemonically as $L_{\text{xxx}}\Delta v_{0.yy}$, where xxx indicates the physical box size in parsecs and 0.yy indicates the value of $v_{\text{rms},i}$ in km s^{-1} .

We use the N-body+smoothed particle hydrodynamics (SPH) code GADGET (Springel, Yoshida & White 2001), as modified by Jappsen et al. (2005) to include sink particles, a prescription to describe collapsed objects without following their internal structure. We use 1.64×10^6 particles for the runs with $L_{\text{box}} = 128 \text{ pc}$, and 3.24×10^6 particles for the run with $L_{\text{box}} = 256 \text{ pc}$. Since the larger-box run contains 8 times more mass than the smaller-box ones but uses only twice as many particles, the minimum resolved mass in the larger-box run is four times larger than in the smaller-box run. Unfortunately, the computing resources available in our cluster did not allow us to further increase the number of particles.

We take as units for the code a mass of $1M_\odot$, a length $\ell_0 = 1 \text{ pc}$ and a velocity $v_0 = 7.362 \text{ km s}^{-1}$, implying a time unit $t_0 = \ell_0/v_0 = 0.133 \text{ Myr}$.

3.2. Sink particles

Sink particles are created when a group of SPH particles become involved in a local collapse event. At that point, the SPH particles are replaced by a sink particle whose internal structure is not resolved anymore. The sink particle inherits the total angular momentum and mass of the SPH particles it replaces, and henceforth moves only in response to its inertia and the gravitational force, although it can continue to accrete SPH particles, should they come sufficiently close to the sink particle.

The creation of a sink particle requires a number of conditions to be satisfied. First, the local density should exceed some user-defined threshold value n_{thr} . If this occurs, then the code computes the total mass and angular momentum of the group of particles above n_{thr} to determine whether they are gravitationally bound. If they are, then they are collectively replaced by the sink. At subsequent times, further SPH particles can be accreted by the sink if they come within an ‘‘accretion radius’’ r_{acc} of the sink and are gravitationally bound to it. In all cases

we use $n_{\text{thr}} = 10^5 \text{ cm}^{-3}$ and $r_{\text{acc}} = 0.04 \text{ pc}$. This value of r_{acc} amounts to roughly 1/3 of the Jeans length at n_{thr} . Due to the limited mass resolution we can afford, the sinks should in general be considered star clusters rather than isolated stars, although some of them may actually correspond to single stars. Nevertheless, with this caveat in mind, we refer to the sinks as ‘‘stars’’ in a generic way.

3.3. Heating and cooling

The gas is subject to heating and cooling functions of the form

$$\Gamma = 2.0 \times 10^{-26} \text{ erg s}^{-1} \quad (3)$$

$$\frac{\Lambda(T)}{\Gamma} = 10^7 \exp\left(\frac{-1.184 \times 10^5}{T + 1000}\right) + 1.4 \times 10^{-2} \sqrt{T} \exp\left(\frac{-92}{T}\right) \text{ cm}^3. \quad (4)$$

These functions are fits to the various heating (Γ) and cooling (Λ) processes considered by Koyama & Inutsuka (2000), as given by equation (4) of Koyama & Inutsuka (2002).⁵ The resulting thermal-equilibrium pressure P_{eq} , defined by the condition $n^2\Lambda = n\Gamma$ is shown in fig. 2 as a function of density. We have abandoned the piecewise power-law fit we have used in all of our previous papers (e.g., Vázquez-Semadeni, Passot & Pouquet 1995; Passot, Vázquez-Semadeni & Pouquet 1995; Vázquez-Semadeni, Passot & Pouquet 1996; Vázquez-Semadeni, Gazol & Scalo 2000; Gazol et al. 2001; Gazol, Vázquez-Semadeni & Kim 2005), including Paper I, mainly because the present fit is applicable at densities typical of molecular gas.

The usual procedure to apply cooling to the hydrodynamic evolution involves the consideration of the cooling rate in the Courant condition to restrict the simulation time step. For the problem at hand, the high densities reached behind the shocks, for example, would imply an exceedingly small time step and the simulation would become computationally unfeasible. But this appears completely unnecessary, because all this means is that the thermal evolution happens faster than the dynamical one, and therefore, as far as the hydrodynamics is concerned, it is instantaneous. Therefore, it is more convenient to use an approximation to the thermal evolution of the gas, which constitutes an extension of that used in Paper I, and which allows us to simply correct the internal energy after the hydrodynamic step has been performed, with no need to adjust the timestep.

Consider the thermal equilibrium temperature, T_{eq} , as a function of the gas density, and the corresponding internal energy density e_{eq} (T_{eq} is a well defined function of the density n as long as $\Lambda(T)$ is monotonic. This is true within the range of temperatures occurring in the simulations). Consider also the time required to radiate the thermal energy excess (if $T > T_{\text{eq}}$; acquire the energy deficit, if $T < T_{\text{eq}}$)

⁵ Note that eq. (4) in Koyama & Inutsuka (2002) contains two typographical errors. The form used here incorporates the necessary corrections, kindly provided by H. Koyama.

$$\tau_\Lambda = \left| \frac{e - e_{\text{eq}}}{n^2 \Lambda - n \Gamma} \right|. \quad (5)$$

Then, we compute the new internal energy density e' , after a time step dt , as

$$e' = e_{\text{eq}} + (e - e_{\text{eq}}) \exp(-dt/\tau_\Lambda). \quad (6)$$

Note that, if the gas is cooling down (or heating up) rapidly, $\tau_\Lambda \ll dt$, $\exp(-dt/\tau_\Lambda) \rightarrow 0$ and the gas immediately reaches its equilibrium temperature, without ever overshooting beyond that value. Conversely, if the gas is at very low density or is close to the equilibrium temperature, $\tau_\Lambda \gg dt$, and equation (6) becomes,

$$e' = e - dt(n^2 \Lambda - n \Gamma), \quad (7)$$

where we, again, use the fact that $\Lambda(T)$, as given by equation (4), is a monotonic function of the temperature.

3.4. Gravitational instability in cooling media

The standard Jeans instability analysis is modified in a medium in which the balance between heating and *instantaneous* cooling produces a net polytropic behavior, characterized by an effective polytropic exponent γ_e , which is the slope of the thermal-equilibrium pressure *versus* density curve (fig. 2). In this case, the Jeans length is found to be given by (e.g., Elmegreen 1991; Vázquez-Semadeni, Passot & Pouquet 1996)

$$L_J \equiv \left[\frac{\gamma_e \pi c^2}{\gamma G \rho_0} \right]^{-1/2}, \quad (8)$$

where c is the adiabatic sound speed and γ is the heat capacity ratio of the gas. Equivalently, this instability criterion can be described as if the effective sound speed in the system were given by $c_{\text{eff}} = \sqrt{\gamma_e k T / \mu}$, where k is Boltzmann's constant and μ is the mean molecular weight. Note that, when $\gamma_e = 0$, the thermal pressure does not react to density changes and therefore is unable to oppose the collapse, rendering the medium gravitationally unstable at all scales ($L_J = 0$). In a more realistic situation where the cooling is not instantaneous, the Jeans length will be limited by the cooling length. In this work, the cooling has a finite characteristic timescale, given by eq. (5).

At the initial uniform density $n_0 = 1 \text{ cm}^{-3}$ and temperature $T_0 = 5000 \text{ K}$, $\gamma_e \sim 0$ and the Jeans length is also near zero. This can be seen in fig. 2, where the vertical dotted line shows the initial uniform density, at which the local tangent to the $P_{\text{eq}} \text{ vs. } \rho$ curve is seen to have a nearly zero slope. However, when the compression produces a dense cloud at the midplane of the box, the rest of the gas decreases its density and enters the fully stable warm phase. For reference, at a density $n = 0.5 \text{ cm}^{-3}$ and a corresponding equilibrium temperature $T_{\text{eq}} = 6300 \text{ K}$, $\gamma_e = 0.834$ and $L_J = 1324 \text{ pc}$, implying a Jeans mass $M_J = 3.47 \times 10^7 M_\odot$. Under these conditions, our runs with $L_{\text{box}} = 128$ and $L_{\text{box}} = 256 \text{ pc}$ would initially contain $\sim 10^{-3}$ and $\sim 10^{-2}$ Jeans masses, respectively.

4. RESULTS

4.1. Mass evolution

In general, the simulations evolve as described in Paper I and in sec. §2. As an illustration, figs. 3 and 4 show selected snapshots of run L256 Δv 0.17 viewed edge-on and face-on, respectively. In the electronic version of the paper, these figures are also available as full-length animations. The times indicated in the frames are in the code's internal unit, $t_0 = 0.133 \text{ Myr}$.

The animation shows that the gas at the collision site begins to undergo a phase transition to the cold phase (the CNM) at roughly one cooling time after the collision (Hennebelle & Pérouault 1999; Vázquez-Semadeni et al. 2006), becoming much denser and colder. Because this gas is in equilibrium with the total (thermal+ram) pressure of the inflow, the density overshoots far beyond that of standard CNM, well into the realm of molecular gas, with mean densities of several hundred cm^{-3} and temperatures of a few tens of Kelvins. This implies a much lower Jeans mass than that in the conditions of the initial WNM and quickly the cloud's mass exceeds its Jeans mass.

Defining the "cloud" as the material with $n > 50 \text{ cm}^{-3}$, the cloud's mass becomes larger than its mean Jeans mass at $t \sim 2.2 \text{ Myr}$ in runs with $L_{\text{box}} = 128 \text{ pc}$ and at $t \sim 3 \text{ Myr}$ in the run with $L_{\text{box}} = 256 \text{ pc}$, at which times the mean density in the dense gas is $\langle n \rangle \sim 65 \text{ cm}^{-3}$, the mean temperature is $\langle T \rangle \sim 50 \text{ K}$, the Jeans mass is $M_J \sim 1200 M_\odot$, and the free-fall time is $\tau_{\text{ff}} \equiv L_J/c \sim 11 \text{ Myr}$, where c is the local sound speed. For comparison, the total mass in the two cylinders, which contain the material that initially builds up the cloud, is $1.13 \times 10^4 M_\odot$ in the runs with $L_{\text{box}} = 128 \text{ pc}$, and $2.26 \times 10^4 M_\odot$ in the run with $L_{\text{box}} = 256 \text{ pc}$. Thus, the cloud eventually becomes much more massive than its mean Jeans mass. For example, in run L256 Δv 0.17 at $t = 17.26 \text{ Myr}$, the (mass-weighted) mean density of the dense gas is $\langle n \rangle \sim 600 \text{ cm}^{-3}$, the mean temperature is $\langle T \rangle \sim 37 \text{ K}$, and $\gamma_e \sim 0.75$. These values imply a mean effective Jeans mass $M_J \sim 300 M_\odot$, while at that time the cloud contains $\sim 2.35 \times 10^4 M_\odot$. Note that the cloud+sink mass might exceed the mass in the inflows, since ambient material surrounding the cylinder is dragged along with the flow, effectively increasing the amount of gas in the inflow (see below).

The animations show that global collapse does indeed occur, although at significantly later times than when the cloud's mass becomes larger than the Jeans mass, probably reflecting the role of turbulence as an opposing agent to the collapse. Indeed, the clouds in the 128-pc boxes begin global contraction at $t \sim 8 \text{ Myr}$, while the cloud in the 256-pc box, with more than twice the inflow duration, begins contracting at $t \sim 12.5 \text{ Myr}$.

Figure 5 (*top* panel) shows the evolution of the cloud's mass in run L256 Δv 0.17, together with the mass in collapsed objects (sinks), to be discussed further in §4.5. It is clearly seen that the *cloud's mass is not constant, but rather evolves in time*. Gas at cloud densities first appears after 2 Myr of evolution, and the cloud's mass increases monotonically until $t \sim 19.5 \text{ Myr}$, at which time it reaches a maximum value $M_{\text{cl}} \sim 2.7 \times 10^4 M_\odot$. After this time, it begins to decrease because of the rapid conversion of gas to stars.

By the end of the simulation, the total mass in stars plus dense gas is almost three times the initial mass in

the inflows. In practice, the inflows last longer than the simple estimate $\tau_{\text{inf}} \equiv \ell_{\text{inf}}/v_{\text{inf}}$ would indicate, and involve more mass than the mass initially within the cylinders. This is due to the fact that, as the cylinders begin advancing, they leave large voids behind them that have the double effect of slowing down the tails of the inflows and of dragging the surrounding gas behind the cylinders. For $v_{\text{inf}} = 9.20 \text{ km s}^{-1}$, $\tau_{\text{inf}} = 5.22 \text{ Myr}$ for runs with $\ell_{\text{inf}} = 48 \text{ pc}$ (L128 Δv 0.24 and L128 Δv 0.66), and $\tau_{\text{inf}} = 12.17 \text{ Myr}$ for the run with $\ell_{\text{inf}} = 112 \text{ pc}$ (L256 Δv 0.17). Instead, in the first two runs, the inflow actually lasts $\sim 11 \text{ Myr}$, while in the latter run it lasts $\sim 22.5 \text{ Myr}$. This can be observed in the animation of fig. 3, in which the velocity field arrows clearly show the gradual decay of the inflows, and their longer duration compared to the simple linear estimate.

4.2. Cloud disruption

Our simulations do not include any feedback from the stellar objects, while this process is probably essential for the energy balance and possibly the destruction of the cloud (e.g., Cox 1983, 1985; Franco, Shore & Tenorio-Tagle 1994; Hartmann, Ballesteros-Paredes & Bergin 2001; Matzner 2002; Nakamura & Li 2005; Li & Nakamura 2006; Mellema et al. 2006). Thus, the simulations cannot be safely considered realistic after their stellar content would likely disrupt the cloud. We now present an *a posteriori* estimation of the time at which this occurs.

Franco, Shore & Tenorio-Tagle (1994) have suggested that the maximum number of OB stars that the cloud can support at any time is given by the number of H II regions required to completely ionize the cloud. In particular, they found that the maximum number of massive stars that can be formed within a molecular cloud is

$$N_{\text{OB,inside}} \simeq \frac{16M_{c,4} n_3^{3/7}}{F_{48}^{5/7} (c_{s,15} t_{\text{MS},7})^{6/7}}, \quad (9)$$

where $M_{c,4}$ is the mass of the cloud, in units of $10^4 M_{\odot}$, n_3 is the number density in units of 10^3 cm^{-3} , F_{48} is the photoionizing flux from the massive stars, in units of 10^{48} s^{-1} , $c_{s,15}$ is the isothermal sound speed in units of 15 km s^{-1} , and $t_{\text{MS},7}$ is a characteristic OB star main sequence lifetime, in units of 10^7 yr . However, as Franco, Shore & Tenorio-Tagle (1994) pointed out, clouds are more efficiently destroyed by stars at the cloud edge because the lower external pressure ensures that the ionized gas expands rapidly away from the cloud, driving a fast ionization front into the dense material. Thus, in this case, these authors find that the maximum number of OB stars that the molecular cloud can support is given by:

$$N_{\text{OB,edge}} \simeq \frac{3M_{c,4} n_3^{1/5}}{F_{48}^{3/5} (c_{s,15} t_{\text{MS},7})^{6/5}}. \quad (10)$$

In order to determine the time at which the MC in our simulation has formed a sufficient number of stars to disrupt it, we proceed as follows. Since the individual sink particles in the simulations in general correspond to

clusters rather than to single stars, we cannot use the sink particle masses directly. Instead, for each temporal output of our simulation, we fit a standard initial mass function (Kroupa 2001) to the total mass in sink particles at that time, to obtain the “real” distribution of stellar masses in the simulation at that time.⁶ We then use Table 1 of Díaz-Miller, Franco & Shore (1998), which gives the ionizing flux as a function of stellar mass, to estimate the flux associated to each mass bin, and then integrate over all relevant masses to obtain the total F_{48} .

Now, from eqs. (9) or (10) one can solve for $M_{c,4}$ as a function of N_{OB} , to find the minimum cloud mass that survives the ionizing radiation from the existing OB stars in the simulation. When this minimum surviving mass is larger than the actual cloud mass, we expect that the cloud will be disrupted. Since we define the “cloud” as the gas with densities above 50 cm^{-3} , we take $n_3 = 0.05$. Also, for simplicity we assume $c_{s,15} t_{\text{MS},7} \sim 1$.

For run L256 Δv 0.17, fig. 6 shows the evolution of the cloud’s mass together with the minimum disrupted cloud mass under the two estimates, eqs. (9) and (10). We see that the cloud is expected to be disrupted at $t = 20.3$ with either estimate.

At this time the mass in sinks is $M_{\text{sinks}} = 5.25 \times 10^3 M_{\odot}$ and the cloud’s mass is $M_{\text{cl}} = 2.67 \times 10^4 M_{\odot}$, so that the star formation efficiency (SFE) up to this time has been

$$\text{SFE} = \frac{M_*}{M_{\text{cl}} + M_*} \approx 16\%. \quad (11)$$

This number is still larger than observational estimates for cloud complexes (Myers et al. 1986), and suggests that additional physical processes, such as longer inflow durations (§4.6) or magnetic fields (§5.2) may be necessary to further reduce the SFE.

We conclude from this section that after $t \approx 20.3 \text{ Myr}$ run L256 Δv 0.17 is probably not realistic anymore, as far as the evolution of a real MC is concerned, and we thus restrict most of our subsequent discussions to times earlier than that, except when later times may be illustrative of some physical process. Self-consistent inclusion of stellar feedback in the simulations, similarly to the studies of Nakamura & Li (2005) and Li & Nakamura (2006), to investigate the final stages of MC evolution will be the subject of future work.

4.3. Turbulence evolution

The collision also generates turbulence in the dense gas, and so the cloud can be considered to be in a driven turbulent regime while the inflows persist, and in a decaying regime after the inflows subside, although the transition from driven to decaying is smooth, rather than abrupt, since the inflows subside gradually, as explained above. Figure 5 (*bottom* panel) shows the evolution of the velocity dispersion σ for the dense gas along each of the three coordinate axes for run L256 Δv 0.17. During the first 10 Myr of the cloud’s existence ($2 \lesssim t \lesssim 12 \text{ Myr}$) $\sigma_y \approx \sigma_z \sim 4 \text{ km s}^{-1}$, although it is interesting to note that the turbulence appears to be anisotropic, with σ_x

⁶ Note that this estimate for the number of massive stars as a function of time is probably a lower limit, as recent simulations suggest that massive stars in clusters tend to form first, while stars formed later tend to be less massive because of the competition for accretion with the existing massive stars (e.g. Bonnell 2005).

first increasing and then decreasing. It reaches a maximum of more than twice as large ($\sim 8.5 \text{ km s}^{-1}$) as that of σ_y and σ_z at $t \approx 6 \text{ Myr}$, reflecting the fact that the inflows are directed along this direction. This suggests that the generation of transverse turbulent motions is not 100% efficient. Of course, this effect is probably exaggerated by our choice of perfectly anti-parallel colliding streams. Clouds formed by obliquely colliding streams are likely to have more isotropic levels of turbulence.

After $t \sim 6 \text{ Myr}$, σ_x begins to decrease, reflecting the weakening of the inflows, settling at $\sigma_x \sim 6 \text{ km s}^{-1}$ by $t \sim 12 \text{ Myr}$. At this time, σ_y and σ_z begin to increase, reflecting the global collapse of the cloud on the yz plane, while σ_x remains nearly stationary, unaffected by the global planar collapse, until $t \sim 18 \text{ Myr}$, at which time it also begins to increase. This coincides with the onset of star formation, and probably reflects the local, small-scale, isotropic collapse events forming individual collapsed objects.

4.4. Evolution of the density, pressure and temperature distributions

An important consideration for understanding the production of local collapse events is the distribution of the density and temperature as the cloud evolves. This is shown in fig. 7, where the normalized mass-weighted histograms of density (*left* panel) and of temperature (*right* panel) are shown at times 4, 8, 12, 14, 16, and 20 Myr for run L256 Δv 0.17. It can be seen that a cold phase already exists at $t = 4 \text{ Myr}$, although at this time the cloud's conditions do not greatly exceed those of the standard CNM, meaning that turbulence is only building up in the cloud at this stage, at which the simulation resembles a two-phase medium. At $t = 8 \text{ Myr}$, the density maxima and temperature minima have shifted to more extreme values, which persist up to $t = 12 \text{ Myr}$, indicating that the density and temperature fluctuations are predominantly created by the supersonic turbulence in the cloud (Vázquez-Semadeni et al. 2006). However, by $t = 14 \text{ Myr}$, the density and temperature extrema are seen to be again moving towards more extreme values, and this trend persists throughout the rest of the simulation, indicating that gravitational collapse has taken over the evolution of the density fluctuations (see also §4.5).

It thus appears that in this particular simulation, the turbulent density fluctuations act as simply as seeds for the subsequent growth of the fluctuations by gravitational instability, as proposed by Clark & Bonnell (2005). However, both in that paper as in the present study, the global turbulence is already decaying, and by definition it cannot then continue competing with self-gravity. Minimally, a fundamental role of turbulence, even in this decaying state, must be to create *nonlinear* density fluctuations, of much larger amplitudes than would be created by thermal instability alone, which can collapse in shorter times than the whole cloud (cf. §§4.5 and 5.1). In any case, simulations in which the inflow lasts beyond the onset of collapse would be desirable, but unfortunately, as mentioned in §4.6, we have not found it feasible to attempt them with the present code and computational resources, and such a study must await a different numerical scheme and physical setup.

4.5. Energy evolution and star formation

Figure 8 (*top* panel) shows the evolution of the kinetic (E_k) and thermal (E_{th}) energies within a cylinder of length 16 pc and radius 32 pc centered at the middle point of the numerical box, together with the evolution of the (absolute value of the) gravitational energy ($|E_g|$) for the entire simulation box. This cylinder contains most of the cloud's mass throughout the simulation, although it also contains sizable amounts of interspersed WNM. Figure 8 (*bottom* panel), on the other hand, shows the evolution of the same energies but with E_k and E_{th} calculated for the dense gas only.

The gravitational energy is shown for the entire box because of the practical difficulty to evaluate it only for the cloud's mass, although we expect the latter to dominate the global gravitational energy when the cloud has become very massive. Indeed, we observe that $|E_g|$ at late times is very large and dominates the other forms of energy. A brief period of positive values of $|E_g|$ is observed for $0 \lesssim t \lesssim 9 \text{ Myr}$, which can be understood as follows: Because the boundary conditions are periodic, Poisson's equation for the gravitational potential is actually modified to have the density fluctuation $\rho - \langle \rho \rangle$ as its source. This is standard fare in cosmological simulations (see, e.g., Alecian & Léorat 1988; Kolb & Turner 1990). Moreover, gravity is a long-range force, and so large-scale features tend to dominate E_g . Thus, during the early epochs of the simulation, when the cloud is beginning to be assembled, the dominant density features are the voids left behind by the cylinders because they are large, while the cloud is small and not very massive. However, once the cloud becomes sufficiently massive, and the voids have been smoothed out, the cloud dominates E_g . The period of positive E_g is omitted from both panels of fig. 8.

Comparison of the energy plots (figs. 8 *top* and *bottom*) with the evolution of the gas and sink masses (fig. 5 *top*) and the animations shows some very important points. First and foremost, the cloud is never in virial equilibrium over its entire evolution. Instead, we can identify three main stages of evolution. First, over the period $8.5 \lesssim t \lesssim 14 \text{ Myr}$, $|E_g|$ increases monotonically, transiting from being negligible compared to E_k and E_{th} to becoming larger than either one of them. The exact time at which this occurs depends on what system is being considered. It occurs at $t \sim 10 \text{ Myr}$ when only the energies in the dense gas are considered, while it occurs at $t \sim 18 \text{ Myr}$ when the entire cylinder, which includes substantial amounts of warm gas, is considered. Since global gravitational contraction starts at $t \sim 12 \text{ Myr}$, it appears that the true balance is bracketed by the estimates based on the full cylinder volume and on the dense gas, though closer to the latter. Thus, over the interval $8.5 \lesssim t \lesssim 12 \text{ Myr}$, the increase in $|E_g|$ is driven mostly by the cooling and compression of the gas.

Second, from $t \sim 12 \text{ Myr}$ to $t \sim 24 \text{ Myr}$, $|E_g|$ continues to increase (E_g becomes more negative), but now driven by the global collapse of the cloud. Over this period, we see that E_k for the dense gas (fig. 8, *bottom* panel) closely follows $|E_g|$, approximately satisfying the condition

$$|E_g| = 2E_k. \quad (12)$$

We see that in this case, *this condition is a signature of*

collapse, not of gravitational equilibrium, even though it lasts for nearly 12 Myr. The maintenance of this equipartition arises from the fact that the cloud is converting gravitational potential energy into kinetic energy, but is replenishing the former by the collapse itself.

Note that we have cautioned in §4.2 that our simulations may not be realistic after $t \approx 20.3$ Myr, because by that time the stellar energy feedback may be sufficient to revert the global collapse and disperse the cloud, but even in that case the cloud will have evolved out of equilibrium up to that point.

Finally, after $t \sim 24$ Myr, the gravitational and kinetic turbulent energies saturate and begin to vary in approximate synchronicity. Although this late stage may not be representative of actual MCs, it is important to understand what is happening in the simulation. The near constancy of $|E_g|$ and E_k could naively be interpreted as a final state of near virial equilibrium. However, inspection of the animations shows otherwise. At $t \sim 24$ Myr, the main body of the cloud is completing its global collapse, and the mass in stars is beginning to exceed the mass in dense gas, which is itself decreasing. So, at this point, the gravitational energy is beginning to be dominated by the stars, rather than by the gas. Moreover, the face-on animation (fig. 4) shows that at this time ($t = 180$ in code units, shown in the animations) the star cluster is beginning to re-expand, after having reached maximum compression. This leads to the decrease of $|E_g|$ between $t \sim 24$ and $t \sim 28$ Myr. Meanwhile, E_k , which is dominated by the dense gas, decreases because the dense gas is being exhausted. Nevertheless, the outer “chaff” of the dense gas, mostly in the form of radial filaments, is continuing to fall onto the collapsed cloud. This leads to a new increase in both energies, as this is a secondary collapse. This situation repeats itself at $t \sim 32$ Myr ($t = 244$ in code units) after the secondary collapse ends and its second-generation star cluster begins to expand away. The end of each collapse and the re-expansion of the clusters is marked by kinks in the graph of M_{sinks} versus time in fig. 5 (*top*), indicating a decrease in the star formation rate.

It is important to recall as well that the condition given by eq. (12) is not sufficient for virial equilibrium. The necessary and sufficient condition for this is that the second time derivative of the moment of inertia of the cloud be zero, and eq. (12) cannot guarantee this, as many other terms enter the full virial balance of the cloud (Ballesteros-Paredes, Vázquez-Semadeni & Scalo 1999; Ballesteros-Paredes 2006; Dib et al 2006). Thus, the observed closeness of $|E_g|$ and E_k in actual molecular clouds must exclusively be considered an indication of near equipartition and probably of collapse, but not of virial equilibrium (see also Klessen et al. 2005).

Thus, rather than evolving in near virial equilibrium, *the cloud evolves far from equilibrium*. $|E_g|$ starts out from essentially zero and increases monotonically until it catches up with the thermal and kinetic energies. From that time on, gravity dominates the energy balance, leading to collapse, which in turn causes a near equipartition between $|E_g|$ and E_k , although both energies continue to vary systematically.

Finally, figure 5 (*top*) also shows that star formation begins at $t \sim 17.2$ Myr, roughly 5 Myr after global contraction of the cloud has begun. Yet, the star-forming

local collapse events proceed much more rapidly than the global collapse of the cloud. This indicates that the turbulence in the cloud has created *nonlinear* density fluctuations, whose local free-fall time is shorter than that of the whole cloud. In particular, the mass in stars increases from zero to $\sim 15\%$ of the cloud’s mass in ~ 3 Myr (from $t = 17$ to $t = 20$ Myr).

The main conclusions from this section are that a) the cloud evolves far from equilibrium all the way from its inception through its final collapse; b) as soon as E_g dominates the dynamics, the cloud develops equipartition indicative of the collapse, not of equilibrium, and c) star formation is rapid in comparison with the evolution and collapse of the whole cloud.

4.6. Effect of the inflow duration and initial velocity dispersion

In previous papers (Vázquez-Semadeni, Kim & Ballesteros-Paredes 2005; Vázquez-Semadeni et al. 2006), it has been argued that the star formation efficiency is a sensitive function of whether the turbulence in the cloud is in a driven or in a decaying regime. Our system is driven at first, and gradually transits to a decaying regime, as pointed out in §4.3. In all of the runs in this paper, global cloud contraction and the subsequent star formation occur after the inflows have weakened substantially ($t > \tau_{\text{inf}}$). The main motivation behind run L256 Δv 0.17 was precisely to model an inflow of as long a duration as possible, to approximate the case of a driven cloud, although this goal was not completely achieved. For example, Hartmann, Ballesteros-Paredes & Bergin (2001) suggest accumulation lengths of up to 400 pc. Runs with even larger boxes (e.g., 512 pc) would be desirable, but they are either prohibitively expensive, or have an excessively poor mass resolution. In addition, vertical stratification effects would have to be considered. This will require a transition to the code Gadget2, which allows for non-cubic boundary conditions and/or inflow boundary conditions, a task we defer to a subsequent paper.

Nevertheless, comparison of the runs with different inflow lengths does shed light on the effect of a longer driving duration. The cloud in run L256 Δv 0.17, whose inflow has $\ell_{\text{inf}} = 112$ pc and lasts ~ 22 Myr (although it begins weakening at $T \sim \tau_{\text{inf}} = 12.2$ Myr), begins contracting at $t \sim 12.5$ Myr and begins forming stars at $t \sim 17$ Myr, while both runs with $\ell_{\text{inf}} = 48$ pc, for which the inflow lasts 11 Myr (begins weakening at $t \sim \tau_{\text{inf}} = 5.2$ Myr), start to contract at $t \sim 8$ Myr (recall that the inflows have the same density and velocity in all runs). Run L128 Δv 0.24 begins forming stars at $t = 15.75$ Myr, and run L128 Δv 0.66 does so at $t = 13.77$ Myr.

These results clearly suggest that a longer inflow duration delays the onset of both global collapse and star formation, in spite of the fact that the cloud formed by it is more massive. This is attributable to the fact that the turbulence in the cloud is continuously driven by the inflow. This is verified by comparing the three components of the velocity dispersion for runs L256 Δv 0.17 and L128 Δv 0.24, respectively shown in fig. 5 (*bottom*) and fig. 9. Both runs show an initial transient peak in σ_x ending at $t \approx 4$ Myr. However, after this transient, σ_x in run L256 Δv 0.17 increases again, reaching a maximum of $\sigma_x \sim 8.5 \text{ km s}^{-1}$, and decreasing afterwards, until it

nearly stabilizes at a value $\sigma_x \sim 6 \text{ km s}^{-1}$ at $t \sim 11.5$ Myr. During this time interval, $\sigma_y \approx \sigma_z \sim 4 \text{ km s}^{-1}$. Instead, in run L128 Δv 0.24, σ_x does not increase again after the initial transient, and remains at a much more moderate level of $\sigma_x \sim 5 \text{ km s}^{-1}$, while $\sigma_y \approx \sigma_z \sim 3 \text{ km s}^{-1}$. Clearly, the turbulence level is significantly higher in the longer-inflow run.

Note that the delay in the onset of global collapse and of local star formation cannot be attributed to the amplitude of the initial velocity fluctuations in the inflow, since runs L128 Δv 0.24 and L256 Δv 0.17, which have comparable amplitudes, differ substantially in these times, while runs L128 Δv 0.24 and L128 Δv 0.66 begin global contraction at almost the same time and differ by only $\sim 15\%$ in the time at which they begin forming stars, in spite of one having more than twice the velocity fluctuation amplitude of the other. This leaves the inflow duration as the sole cause of delay of both the global and local collapses.

4.7. Local column density and star formation

The initial conditions in our simulations are assumed to consist exclusively of atomic gas. However, the final density and temperature conditions are typical of molecular clouds, so molecule formation must occur somewhere along the way in the evolution of the clouds. One important shortcoming of our simulations is that they cannot distinguish between atomic and molecular gas, as no chemistry is included. Thus, we cannot directly tell from the simulations how long does it take for star formation to begin after molecular gas forms. We can, nevertheless, measure the column density of the dense gas in star-forming regions, and compare it to the estimates for self-shielding given by Franco & Cox (1986) and Hartmann, Ballesteros-Paredes & Bergin (2001), under solar Galactocentric conditions of the background UV field. The former authors find a threshold column density for self-shielding of $N_{\text{ss}} \sim 5 \times 10^{20} \text{ cm}^{-2}$, while the latter authors quote values $N_{\text{ss}} \sim 1\text{--}2 \times 10^{21} \text{ cm}^{-2}$ from van Dishoeck & Black (1988) and van Dishoeck & Blake (1998). So, we take a reference value of $N_{\text{ss}} = 10^{21} \text{ cm}^{-2}$.

For comparison, in Table 2 we report the column densities of the dense gas in the first four regions of star formation in run L256 Δv 0.17 at the time immediately before they begin forming stars. We see that the column densities fall in the range $0.5\text{--}2 \times 10^{21} \text{ cm}^{-2}$, suggesting that star formation *locally* occurs nearly simultaneously with the conversion of the gas from atomic to molecular.

Moreover, we can compare the time at which we expect the bulk of the cloud to become molecular (i.e., the time at which the mean column density in the cloud is reaching N_{ss}) with the time at which star formation begins in the cloud. A lower limit for the time at which the mean column density in the cloud equals N_{ss} is given by

$$t_{\text{ss}} \gtrsim \frac{N_{\text{ss}}}{2n_0 v_{\text{inf}}} = \frac{N_{\text{ss}}}{5.8 \times 10^{19} \text{ cm}^{-2}} \text{ Myr}, \quad (13)$$

where n_0 and v_{inf} have been defined in §3.1. This estimate is a lower limit because, as mentioned in §4.1, v_{inf} is not constant, but actually decreases in time. For $N_{\text{ss}} = 10^{21} \text{ cm}^{-2}$, we obtain $t_{\text{ss}} \gtrsim 17.3$ Myr, suggesting

that the bulk of the cloud is still expected to be predominantly atomic by the time star formation is beginning.

Together, these simple estimates suggest that stars form roughly simultaneously with the conversion of gas from atomic to molecular, with the local star forming regions being more advanced in the conversion process than the bulk of the cloud. In turn, this suggests that our model cloud would be observed as a collection of predominantly molecular clumps immersed in a large, predominantly atomic, substrate. This suggestion is consistent with recent observations that substantial amounts of atomic gas coexist with the molecular phase in MCs (Li & Goldsmith 2003; Goldsmith & Li 2005; Klaassen et al. 2005), with perhaps even warm gas mixed in (Hennebelle & Inutsuka 2006). Of course, a more conclusive confirmation of these estimates must await simulations in which the chemistry and radiative transfer are properly taken care of.

5. DISCUSSION

5.1. Implications

5.1.1. Dynamic evolution and global versus local collapse

The results presented in §4 provide general support to the scenario outlined in Elmegreen (1993b); Ballesteros-Paredes, Vázquez-Semadeni & Scalo (1999); Ballesteros-Paredes, Hartmann & Vázquez-Semadeni (1999); Hartmann, Ballesteros-Paredes & Bergin (2001); Vázquez-Semadeni, Ballesteros-Paredes & Klessen (2003); Hartmann (2003); Mac Low & Klessen (2004); Heitsch et al. (2005, 2006); Vázquez-Semadeni et al. (2006); Ballesteros-Paredes et al. (2006). The clouds in our simulations are never in a state of virial equilibrium before they convert most of their mass into stars. Instead, they are in a continuously evolving state, initially obtaining their mass and turbulence simultaneously as they form out of the compression and cooling of diffuse warm gas (see also Hennebelle & Pérault 1999, 2000; Koyama & Inutsuka 2002; Inutsuka & Koyama 2004). The gas initially has negligible self-gravity compared to its thermal support, but it quickly becomes super-Jeans because of the compression, the cooling, and the mass increase of the dense gas, until its self-gravitating energy eventually becomes comparable with the sum of its thermal and turbulent energies, at which point it begins to undergo global collapse. After this time, gravity becomes the main driver of the large-scale motions in these (semi-) decaying simulations, causing a near-equipartition, $|E_{\text{g}}| \sim 2E_{\text{k}}$, which however is indicative of *collapse*, not equilibrium.

The nonlinear density fluctuations induced by the turbulence collapse faster than the whole cloud, as they have shorter free-fall times, and star formation proceeds vigorously before global collapse is completed. This result is in contrast with the standard notion that *linear* density fluctuations cannot lead to fragmentation because the fastest growing mode of gravitational instability in a nearly uniform medium is an overall contraction of the whole medium (Larson 1985). Thus, a crucial role of the turbulence in the medium is to create *nonlinear* density fluctuations that have shorter free-fall times than the entire cloud.

These results bring back the scenario of global cloud collapse proposed by Goldreich & Kwan (1974),

but with a twist that avoids the criticism of Zuckerman & Palmer (1974), namely that MCs could not be in global collapse because the star formation rate would be exceedingly high. Our simulations suggest that MCs may be undergoing global gravitational contraction, but the efficiency is reduced because local collapse events, which involve only a fraction of the total cloud mass, proceed faster than the global collapse. Once a sufficiently large number of stars have formed, their energy feedback may partially or completely halt the collapse. Further reduction may be provided by supercritical magnetic fields (Vázquez-Semadeni, Kim & Ballesteros-Paredes 2005; Nakamura & Li 2005). This scenario is consistent with the recent proposal of Hartmann & Burkert (2006) that the Orion A cloud may be undergoing gravitational collapse on large scales.

5.1.2. *Cloud’s mass variation and cloud boundaries*

The fact that the cloud’s mass is not constant is equivalent to the property that the locus of a Lagrangian boundary of the cloud defined (by means of a threshold density) at any given time does not remain at the cloud’s boundary as time progresses, but instead it is later incorporated into the interior of the cloud. This implies that the cloud does not always consist of the same set of fluid parcels, and that in a virial balance analysis of the cloud, there is non-zero flux of the physical variables through Eulerian boundaries defined at any given time (Ballesteros-Paredes, Vázquez-Semadeni & Scalo 1999; Shadmehri, Vázquez-Semadeni & Ballesteros-Paredes 2002; Dib et al 2006; Ballesteros-Paredes 2006).

5.1.3. *Absence of slow, accelerating star formation phase*

It is important to note that the star formation rate (given by the slope of the mass in sinks *versus* time in fig. 5 [top]) is large from the start, and we observe no long period of slow, accelerating star formation, contrary to the suggestion of Palla & Stahler (2000, 2002) that star formation accelerates in time. Problems with this suggestion have been discussed by Hartmann (2003), and, within the framework of their assumptions and limitations, our simulations do not confirm it. An important question is whether this result will persist when magnetic fields are included. It is possible that during the early stages of the cloud’s evolution, it may behave under magnetically subcritical conditions, giving very low star formation rates (SFRs), and then transit into a supercritical regime, with higher SFRs (§5.1.5).

5.1.4. *Latency period*

The clouds in our simulations do spend a long latency period between the beginning of the compressive motion that creates the cloud and the time at which they begin forming stars ($\sim 14\text{--}17$ Myr in the three runs we have considered). However, this long period is most probably spent in the atomic phase, since the column densities of the star-forming regions in the simulations are comparable to those required for molecule formation (Franco & Cox 1986; Hartmann, Ballesteros-Paredes & Bergin 2001). More specifically, Bergin et al. (2004) have found that the timescale for CO molecule formation is essentially that required for reaching a dust extinction of $A_V \sim$

0.7. Note also that during this time, the formation of H_2 can be fast within density peaks (cores), even if most of the mass of the cloud is still in the low-density regime (Pavlovski et al. 2002; Glover & Mac Low 2006). Thus, the concept of “rapid” star formation refers to the time elapsed between the appearance of a (CO) molecular cloud and the onset star formation, as well as to the *rate* of the star formation process itself.

Note that the latency period is in fact by definition of the order of the crossing time of the entire large-scale compressive wave, in agreement with observational evidence (Elmegreen 2000).

5.1.5. *Implications for HI envelopes and magnetic criticality*

The formation of GMCs by an accumulation process such as the one modeled here has two important additional implications. First, because the process starts with lower-density gas (the WNM in our simulations) that is compressed by some external agent, GMCs, which are the “tip of the iceberg” of the density distribution, are expected to have in general HI envelopes, which would constitute the corresponding “body of the iceberg”. This gas would include transition material traversing the unstable phase between the warm to the cold phases, which would appear to have a nearly isobaric behavior (Gazol, Vázquez-Semadeni & Kim 2005; Audit & Hennebelle 2005; Vázquez-Semadeni et al. 2006), in agreement with the conclusion reached by Andersson & Wannier (1993) from observations of HI envelopes of MCs. Such envelopes are routinely observed (e.g., Blitz & Thaddeus 1980; Wannier Lichten & Morris; Andersson, Wannier & Morris 1991; Andersson & Wannier 1993; Ballesteros-Paredes, Hartmann & Vázquez-Semadeni 1999; Brunt 2003; Blitz et al. 2006, see also the combined HI and CO maps of Blitz & Rosolowsky 2004). Weaker compressions than we have modeled may produce mostly thin CNM sheets, with little or no molecular gas, as discussed in Vázquez-Semadeni et al. (2006).

Second, this scenario of molecular cloud formation implies that the mass-to-flux ratio of the cloud is a variable quantity as the cloud evolves. This ratio is equivalent to the ratio of column density to magnetic field strength (Nakano & Nakamura 1978), with the critical column density given by $\Sigma \sim 1.5 \times 10^{21} [B/5\mu G] \text{ cm}^{-2}$. Although in principle under ideal MHD conditions the criticality of a magnetic flux tube involves *all* of the mass contained within it, in practice it is only the mass in the dense gas phase that matters, because the diffuse gas is not significantly self-gravitating at the size scales of MC complexes. As pointed out by Hartmann, Ballesteros-Paredes & Bergin (2001), the above value of the dense gas’ column density for magnetic criticality is very close to that required for molecule formation (eq. [1]) and for gravitational binding (eq. [2]), and therefore, the cloud is expected to become magnetically supercritical nearly at the same time it is becoming molecular and self-gravitating.

5.2. *Limitations and future work*

Our simulations are limited in a number of aspects. First and foremost, as already mentioned in §3.2, one

major shortcoming of our simulations is the absence of feedback from the stellar objects onto the cloud. This is certainly an unrealistic feature. Second, our clouds are in a regime of turbulence decay after the inflows have subsided. This may or may not be an unrealistic feature, and rather it may represent a fraction of the population of clouds. Finally, we have neglected magnetic fields altogether, due to the non-existence of suitable SPH algorithms including MHD for the problem of fully developed turbulent flows.

All of these limitations tend to exaggerate the SFE in our simulations, as the turbulence within them is not replenished by either a continuing flow or by stellar energy feedback. It is possible that a continued inflow (and therefore a sustained turbulence level) could prevent global collapse altogether, with only local collapse events happening randomly, although certainly the inflows cannot last indefinitely. Thus, it would appear that global collapse is inescapable. However, once star formation begins, the stellar energy feedback is likely to either be able to halt the global collapse and disperse the cloud (Franco, Shore & Tenorio-Tagle 1994; Hartmann, Ballesteros-Paredes & Bergin 2001) or else maintain it in rough equilibrium (e.g., Matzner 2002; Nakamura & Li 2005; Tan, Krumholz & McKee 2006; Krumholz, Matzner & McKee 2006). Thus, two important questions to address in future papers are, one, what is the evolution like when star formation begins before the inflows subside. It is likely that this case will have much smaller SFEs. Two, whether the stellar energy feedback tends to disperse the clouds, or else to maintain them in rough equilibrium. Observationally, star clusters older than 5–10 Myr tend to be already devoid of gas (Leisawitz, Bash & Thaddeus 1989; Hartmann, Ballesteros-Paredes & Bergin 2001; Ballesteros-Paredes & Hartmann 2006), suggesting that the effect is more disruptive than equilibrating.

Finally, our simulations have neglected the magnetic field. As discussed in §2, this is not a crucial omission if GMCs are in general magnetically supercritical, since the supercritical case is qualitatively equivalent to the nonmagnetic case, with the only difference being that it behaves as if it were less massive than a non-magnetic cloud of the same mass (Shu 1992; Hartmann 1998). Thus, we consider that our models are still representative of the large-scale evolution up to the early times of star formation in supercritical clouds. The main difference is expected to be that magnetized, supercritical clouds should have lower SFEs than nonmagnetic ones (Vázquez-Semadeni, Kim & Ballesteros-Paredes 2005; Nakamura & Li 2005). On the other hand, the evolution of subcritical clouds will certainly differ from the models presented here, because they will have no global tendency to collapse. At any rate, it is necessary to perform simulations of the full process in the presence of magnetic fields. This will presumably require the usage of AMR techniques incorporating the analogue of sink particles and stellar feedback, and will be pursued in future papers.

6. SUMMARY AND CONCLUSIONS

In this paper we have presented a suite of numerical simulations designed to investigate jointly the formation of molecular clouds (MCs) and of stars within

them. The simulations use an SPH scheme including self-gravity, sink particles and cooling leading to thermal bistability. Magnetic fields are neglected. The simulations describe the collision of oppositely-directed gas streams (“inflows”) in the warm neutral medium (WNM) at moderately supersonic velocities (each with a velocity of 9.2 km s^{-1} , or a Mach number of 1.22 in the unperturbed WNM). Three simulations were considered, varying the length of the inflow and the amplitude of the initial velocity fluctuations in the gas. The collisions trigger a transition to the cold phase in the gas, and simultaneously generate turbulence in the resulting “cloud”, defined as the gas at densities $n > 50 \text{ cm}^{-3}$. The inflows secularly weaken in time, and so does the turbulence level in the cloud, implying that the turbulence in the clouds gradually transits from being continuously driven to being in a decaying regime. The cooling and the mass gain of the dense gas eventually cause the cloud to contain a large number of Jeans masses at the mean conditions. Moreover, because the cloud is supersonically turbulent, locally the density can be much larger, with a correspondingly lower Jeans mass and shorter free-fall times than those of the whole cloud.

Thus, by the time the inflows have almost subsided, the cloud engages in global gravitational collapse, but shortly thereafter it begins to produce numerous local collapse events that occur on much smaller timescales because of the larger densities, so that by the time the global collapse of the cloud is completed, it has converted most of its mass to collapsed objects (sink particles). The sinks in general represent star clusters, due to the limited mass resolution and lack of modeling of opacity-limited fragmentation (e.g. Bate, Bonnell & Bromm 2003). Our simulations can only be considered reliable up to the time when the mass in collapsed objects (sinks) implies a high enough number of massive stars that they would disrupt the cloud. Nevertheless, the evolution up to that point shows a number of relevant results:

1. The clouds are never in virial equilibrium during this period. Instead, they continually evolve, increasing their mass and self-gravitating energy, until the latter becomes comparable or larger than the thermal and kinetic energies. Some ~ 5 Myr after global contraction began, star formation begins.
2. In spite of not being in equilibrium, the near-equipartition condition $|E_g| \sim 2E_k$ is approximately satisfied as soon as $|E_g|$ becomes comparable to E_k , because of the gravitational contraction of the cloud, with both quantities increasing simultaneously. This occurs long before the onset of star formation. This fact can explain the observed state of apparent virialization of GMCs.
3. The near equipartition is a signature of global gravitational collapse, not equilibrium, and suggests a return to Goldreich & Kwan’s (1974) scenario of global gravitational contraction in MCs. However, the criticism by Zuckerman & Palmer (1974), namely that an excessively large star formation should result through this process, is avoided in part because the nonlinear turbulent density fluctuations collapse earlier than the whole cloud, involving only a fraction of the total mass, and in part because as soon as the stars form they probably contribute to dispersing the cloud, or at least halting its global col-

lapse. Further reduction of the SFE may occur in the presence of supercritical magnetic fields.

4. Local collapse events begin to occur after global collapse has begun, but they occur rapidly, requiring only ~ 3 Myr to convert $\sim 15\%$ of the cloud's mass into stars.
5. The star formation rate, measured by the slope of the mass in stars *versus* time, is large from the beginning. Within the framework, assumptions and limitations of our simulations, no long period of slow, accelerating star formation is observed.
6. Longer inflow durations maintain larger turbulent velocity dispersions in the clouds and delay the onset of both global and local collapse. Instead, larger amplitudes of the initial velocity fluctuations have little effect in delaying the collapse. The latter effect can be attributed to the fact that the turbulence is already dissipating in the clouds by the time global collapse begins.
7. A long period (~ 14 – 17 Myr) of “dormancy” does occur between the time when the cloud begins to form and the time when star formation begins. Nevertheless, it is likely that most of this time is spent with the gas being in atomic form, since the column density of star forming regions in our simulations are comparable to values required for molecular gas formation, as reported in the literature. Thus, our simulations support the notion that star formation occurs almost simultaneously with the formation of molecular gas, under local ISM conditions.

We conclude that our simulations support the

scenario of rapid star formation after molecular gas has formed, involving accumulations of gas from distances of a few hundred parsecs (Hartmann, Ballesteros-Paredes & Bergin 2001; Vázquez-Semadeni, Ballesteros-Paredes & Klessen 2003), while simultaneously requiring timescales of the order of the crossing time across the largest scales involved (Elmegreen 2000), and in a systematically out-of-equilibrium fashion (Ballesteros-Paredes, Vázquez-Semadeni & Scalo 1999; Ballesteros-Paredes, Hartmann & Vázquez-Semadeni 1999; Klessen, Heitsch & Mac Low 2000). However, the evidence will have to be made more compelling as additional physical processes, such as longer-duration inflows, stellar feedback, magnetic fields and chemistry are included.

We thankfully acknowledge useful comments from Lee Hartmann and Chris McKee, and the help of Luis Ballesteros-Paredes with postprocessing of the computer animations. This work has received financial support from CRyA-UNAM; from CONACYT grants 36571-E and 47366-F to E. V.-S., and UNAM-PAPIIT grant 110606; and from the Emmy Noether Program of the German Science Foundation (DFG) under grant Kl1358/1 to R.S.K. and A.K.J. The simulations were performed in the cluster at CRyA-UNAM acquired with grant 36571-E. This work has made extensive use of NASA's ADS and LANL's astro-ph abstract services.

REFERENCES

- Alecian, G. & Léorat, J. 1988, *A&A* 196, 1
- Andersson, B. G., Wannier, P. G., & Morris, M. 1991, *ApJ* 366, 464
- Andersson, B. G., & Wannier, P. G. 1993, *ApJ* 402, 585
- Audit, E. & Hennebelle, P. 2005, *A&A* 433, 1
- Ballesteros-Paredes, J., Hartmann, L. & Vázquez-Semadeni, E. 1999, *ApJ* 527, 285
- Ballesteros-Paredes, J. & Hartmann, L. 2006, *RMAA*, submitted (astro-ph/0605268)
- Ballesteros-Paredes, J., Vázquez-Semadeni, E., & Scalo, J. 1999, *ApJ*, 515, 286
- Ballesteros-Paredes, J., Klessen, R. S., Mac Low, M.-M., Vázquez-Semadeni, E. 2006, in *Protostars and Planets V*, eds. B. Reipurth, D. Jewitt, K. Keil (Tucson: Univ. of Arizona Press), in press (astro-ph/0603357)
- Ballesteros-Paredes, J. 2006, *ApJ*, submitted (astro-ph/0606071)
- Bonnell, I. A., Bate, M. R. 2006, *MNRAS* 370, 488
- Bate, M. R., Bonnell, I. A., & Bromm, V. 2003, *MNRAS* 339, 577
- Bergin, E. A., Hartmann, L. W., Raymond, J. C. & Ballesteros-Paredes, J., 2004, *ApJ* 612, 921
- Blitz, L., & Thaddeus, P. 1980, *ApJ* 241, 676
- Blitz, L. & Shu, F. H. 1980, *ApJ* 238, 148
- Blitz, L. & Williams, J. P. 1999, in *The Origin of Stars and Planetary Systems*, ed. C. J. Lada and N. D. Kylafis (Dordrecht: Kluwer), 3
- Blitz, L. & Rosolowsky, E. 2004 in *IMF@50: The Initial Mass Function 50 Years Later*, eds. E. Corbelli, F. Palla, and H. Zinnecker (Dordrecht: Springer), p. 287
- Blitz, L., Fukui, Y., Kawamura, A., Leroy, A., Mizuno, N., & Rosolowsky, E., 2006, in *Protostars and Planets V*, eds. B. Reipurth, D. Jewitt, K. Keil (Tucson: Univ. of Arizona Press), in press (astro-ph/0602600)
- Bonnell, I. A., Bate, M. R., Clarke, C. J., & Pringle, J. E. 1997, *MNRAS* 285, 201
- Bonnell, I. A., Bate, M. R., Clarke, C. J., & Pringle, J. E. 2001, *MNRAS* 323, 785
- Bonnell, I. 2005, in *Massive star birth: A crossroads of Astrophysics*, IAU Symposium 227, eds. R. Cesaroni, R., M. Felli, E. Churchwell. and M. Walmsley, (Cambridge: Cambridge University Press, 2005.), p.266
- Bonnell, I. A., Dobbs, C. L., Robitaille, T. R., & Pringle, J. E. 2006, *MNRAS*, 365, 37
- Bourke, T. L., Myers, P. C., Robinson, G., Hyland, A. R. 2001, *ApJ* 554, 916
- Brunt, C. M., 2003, *ApJ*, 583, 280
- de Jong, T., Boland, W., & Dalgarno, A. 1980, *A&A* 91, 68
- Clark, P.C. & Bonnell, I.A. 2005, *MNRAS* 361, 2
- Cox, D. P. 1983, *ApJ* 265, L61
- Cox, D. P. 1985, *ApJ* 288, 465
- Crapsi, A., Devries, C. H., Huard, T. L., Lee, J.-E., Myers, P. C., Ridge, N. A., Bourke, T. L., Evans, N. J., II, Jørgensen, J. K., Kauffmann, J., Lee, C. W., Shirley, Y. L., Young, C. H. 2005, *A&A*, 439, 1023
- Crutcher, R. M. 1999, *ApJ* 520, 706
- Crutcher, R., Heiles, C. & Troland, T. 2003, in *Turbulence and Magnetic Fields in Astrophysics*. ed. E. Falgarone, and T. Passot. (Dordrecht: Springer), p. 155
- Díaz-Miller, R. I., Franco, J. & Shore, S. N. 1998, *ApJ* 501, 192
- Dib, S., Vázquez-Semadeni, E., Kim, J., Burkert, A., & Shadmehri, M. 2006, *ApJ*, submitted (astro-ph/0607362)
- Dobbs, C. L., Bonnell, I. A., & Pringle, J. E. 2006, *MNRAS*. 37, .1663
- Elmegreen, B. G. 1985, in *Protostars and Planets II*, (Tucson: University of Arizona Press) p. 33
- Elmegreen, B. G. 1991, in *The Physics of Star Formation and Early Stellar Evolution*, ed. C.J. Lada and N. D. Kylafis (Dordrecht: Kluwer), 35
- Elmegreen, B. G. 1993, in *Protostars and Planets III*, (Tucson: University of Arizona Press) p. 97
- Elmegreen, B. G. 1993, *ApJ* 419, L29
- Elmegreen, B. G. 2000, *ApJ* 530, 277
- Field, G. B., 1965, *ApJ* 142, 531

- Field, G. B., Goldsmith, D. W., & Habing, H. J. 1969, *ApJ*, 155, L149
- Folini, D. & Walder, R. 2006, *A&A*, in press (astro-ph/0606753)
- Franco, J. & Cox, D. P. 1986, *PASP* 98, 1076
- Franco, J. Shore, S. N., & Tenorio-Tagle, G. 1994, *ApJ* 436, 795
- Gazol, A., Vázquez-Semadeni, E., Sañchez-Salcedo, F. J., & Scalo, J. 2001, *ApJ* 557, L121
- Gazol, A. Vázquez-Semadeni, E. & Kim, J. 2005, *ApJ* 630, 911
- Glover, S. C. O. & Mac Low, M.-M. 2006 (astro-ph/0605121)
- Goldreich, P. & Kwan, J. 1974, *ApJ* 189, 441
- Goldsmith, P. F. & Li, D. 2005, *ApJ* 622, 938
- Hartmann, L. 1998, *Accretion Processes in Star Formation* (Cambridge: Cambridge University Press)
- Hartmann, L. 2003, *ApJ* 585, 398
- Hartmann, L., Ballesteros-Paredes, J., & Bergin, E. A. 2001, *ApJ*, 562, 852
- Hartmann, L. & Burkert, A. 2006, *ApJ* submitted
- Heiles, C. & Troland, T. H. 2003, *ApJ*, 586, 1067
- Heiles, C. & Troland, T. H. 2005, *ApJ* 624, 773
- Heitsch, F., Mac Low, M. M., & Klessen, R. S. 2001, *ApJ*, 547, 280
- Heitsch, F., Burkert, A., Hartmann, L., Slyz, A. D. & Devriendt, J. E. G. 2005, *ApJ* 633, L113
- Heitsch, F., Slyz, A. D., Devriendt, J. E. G., Hartmann, L. W., Burkert, A. 2006, *ApJ* submitted (astro-ph/0605435)
- Hennebelle, P., & Pérault, M. 1999, *A&A*, 351, 309
- Hennebelle, P., & Pérault, M. 2000, *A&A*, 359, 1124
- Hennebelle, P. & Inutsuka, S.-I. 2006, *ApJ*, in press (astro-ph/0510389)
- Hunter, J. H., Jr., Sandford, M. T., II, Whitaker, R. W., Klein, R. I. 1986, *ApJ*, 305, 309
- Inutsuka, S.-I. & Koyama, H. 2004, *RMAA*, Ser. Conf. 22, 26
- Jappsen, A.-K., Klessen, R. S., Larson, R. B., Li, Y., and Mac Low, M.-M. 2005, *ã435*, 611
- Klaassen, P. D., Plume, R., Gibson, S. J., Taylor, A. R., Brunt, C. M. 2005, *ApJ* 631, 1001
- Klessen, R. S. 2001a, *ApJ* 550, L77
- Klessen, R. S. 2001b, *ApJ* 556, 837
- Klessen, R. S., Bate, M R. & Burkert, A. 1998, *ApJ*, 501, L205
- Klessen, R. S., Heitsch, F., & MacLow, M. M. 2000, *ApJ*, 535, 887
- Klessen, R. S. & Burkert, A. 2000, *ApJS*, 128, 287
- Klessen, R. S. & Burkert, A. 2001, *ApJ* 549, 386
- Klessen, R. S., Ballesteros-Paredes, J., Vázquez-Semadeni, E., Durán-Rojas, C. 2005, *ApJ* 620, 786
- Kolb, E. W. & Turner, M. S. 1990, *The Early Universe* (Addison-Wesley)
- Koyama, H. & Inutsuka, S.-I. 2000, *ApJ* 532, 980
- Koyama, H. & Inutsuka, S.-I. 2002, *ApJ*, 564, L97
- Kritsuk, A. G. & Norman, M. L. 2002, *ApJ* 569, L127
- Kroupa, P. 2001, *MNRAS* 322, 231
- Krumholz, M. R., McKee, C. F., Klein, R. I. 2005, *Nature*.438, 332
- Krumholz, M. R., Matzner, C. D., McKee, C. F. 2006, *ApJ*, in press (astro-ph/0608471)
- Kulkarni, S. R. & Heiles, C. 1987, in *Interstellar Processes*, ed. D. J. Hollenbach & H. A. Thronson (Dordrecht: Reidel), 87
- Lada, C. J. & Lada, E. A. 2003, *ARA&A* 41, 57
- Larson, R. B. 1985, *MNRAS* 214, 379
- Leisawitz, D., Bash, F. N., & Thaddeus, P. 1989, *ApJS*, 70, 731
- Li, D. & Goldsmith, P. F. 2003, *ApJ* 585, 823
- Li, Z.-Y. & Nakamura, F. 2006, *ApJ* 640, L187
- Matzner, C. D. 2002, *ApJ* 566, 302
- Mac Low, M.-M., & Klessen, R. S. 2004, *Rev. Mod. Phys.* 76, 125
- McKee, C. F. 1999, in *The Origin of Stars and Planetary Systems*, ed. C. J. Lada and N. D. Kylafis (Dordrecht:Kluwer), p.29
- McKee, C. F., Zweibel, E. G., Goodman, A. A., & Heiles, C. 1993, in *Protostars and Planets III*, ed. E. H. Levy & Jonathan I. Lunine (Tucson: University of Arizona Press), 327
- Mellema, G., Arthur, S. J., Henney, W. J., Iliev, I. T. & Shapiro, P. R. 2006, *ApJ* in press (astro-ph/0512554)
- Mouschovias, Tassis & Kunz 2006, *ApJ* 646, 1043
- Myers, P. C., Dame, T. M., Thaddeus, P., Cohen, R. S., Silverberg, R. F., Dwek, E. & Hauser, M. G. 1986, *ApJ* 301, 398
- Nakamura, F. & Li, Z.-Y. 2005, *ApJ* 631, 411
- Nakano, T. & Nakamura, T. 1978, *PASJ* 30, 671
- Palla, F. & Stahler, S. W., 2000, *ApJ* 540, 255
- Palla, F. & Stahler, S. W., 2002, *ApJ* 581, 1194
- Pavlovski, G., Smith, M. D., Mac Low, M.-M., and Rosen, A. 2002, *MNRAS*, 337, 477
- Passot, T., Vázquez-Semadeni, E. & Pouquet, A. 1995, *ApJ* 455, 536
- Rho, J., Reach, W. T., Lefloch, B., Fazio, G. G. 2006, *ApJ*, 643, 965
- Shadmehri, M., Vázquez-Semadeni, E. & Ballesteros-Paredes, J. 2002, in *Seeing Through the Dust: The Detection of HI and the Exploration of the ISM in Galaxies*, ed. A. R. Taylor, T. L. Landecker, and A. G. Willis. (San Francisco: Astronomical Society of the Pacific), p.190
- Shu, F. 1992, *The Physics of Astrophysics, II. Gas Dynamics* (Mill Valley: University Science Books)
- Springel, V., Yoshida, N., White, S. D. M. 2001, *New Astron.* 6, 79
- Tan, J., Krumholz, M. R., & McKee, C. F. 2006, *ApJ*, 641, L121
- Tassis, K. & Mouschovias, T. Ch. 2004, *ApJ* 616, 283
- Tilley, D. A. & Pudritz, R. E. 2004, *MNRAS* 353, 769
- Tilley, D. A. & Pudritz, R. E. 2005, *MNRAS*, submitted (astro-ph/0508562)
- van Dishoeck, E. F. & Black, J. H. 1988, *ApJ* 334, 771
- van Dishoeck, E. F. & Blake, G. A. 1998, *ARA&A* 36, 317
- Vázquez-Semadeni, E., Passot, T. & Pouquet, A. 1995, *ApJ* 441, 702
- Vázquez-Semadeni, E., Passot, T. & Pouquet, A. 1996, *ApJ* 473, 881
- Vázquez-Semadeni, E., Gazol, A., & Scalo, J. 2000, *ApJ*, 540, 271
- Vázquez-Semadeni, E., Ballesteros-Paredes, J. & Klessen, R. 2003, *ApJ*, 585, L131
- Vázquez-Semadeni, E., Kim, J. & Ballesteros-Paredes, J. 2005, *ApJ*, 630, L49
- Vázquez-Semadeni, E., Ryu, D., Passot, T., González, R. F., & Gazol, A., 2006, *ApJ*, 643, 245
- Vishniac, E. T. 1994, *ApJ*, 428, 186
- Walder, R. & Folini, D. 1998 *A&A*, 330, L21
- Walder, R. & Folini, D. 2000, *ApSS*, 274, 343
- Wannier, P. G., Lichten, S. M., Morris, M. 1983, *ApJ*, 268, 727
- Zuckerman, B. & Palmer, P. 1974, *ARA&A*, 12, 279

TABLE 1
RUN PARAMETERS.

Run name	$L_{\text{box}}^{\text{a}}$ (pc)	$\ell_{\text{inf}}^{\text{b}}$ (pc)	$v_{\text{inf}}^{\text{c}}$ (km s $^{-1}$)	$\mathcal{M}_{\text{inf}}^{\text{d}}$	$v_{\text{rms},i}^{\text{e}}$ (km s $^{-1}$)	$M_{\text{box}}^{\text{f}}$ (M_{\odot})	$N_{\text{part}}^{\text{g}}$	ΔM^{h} (M_{\odot})
L128 Δv 0.24	128	48	9.20	1.22	0.24	6.582×10^4	1.643×10^6	0.04
L128 Δv 0.66	128	48	9.20	1.22	0.66	6.582×10^4	1.643×10^6	0.04
L256 Δv 0.17	256	112	9.20	1.22	0.17	5.253×10^5	3.242×10^6	0.16

^a Physical size of computational domain.

^b Linear size of each inflow.

^c Speed of inflows.

^d Mach number of inflows, with respect to sound speed of unperturbed WNM.

^e One-dimensional rms speed of initial imposed velocity fluctuations.

^f Total mass in the computational domain.

^g Number of SPH particles.

^h Mass resolution, equal to the mass of each SPH particle.

TABLE 2
COLUMN DENSITIES OF STAR FORMING REGIONS IN RUN L256 Δv 0.17.

Region	Time (Myr)	Position in yz plane (pc)	N (cm $^{-2}$)
1	17.0	(144,135)	9.58×10^{20}
2	17.26	(131,142)	2.27×10^{21}
3	18.06	(112,125)	4.89×10^{20}
4	18.59	(137,115)	1.52×10^{21}

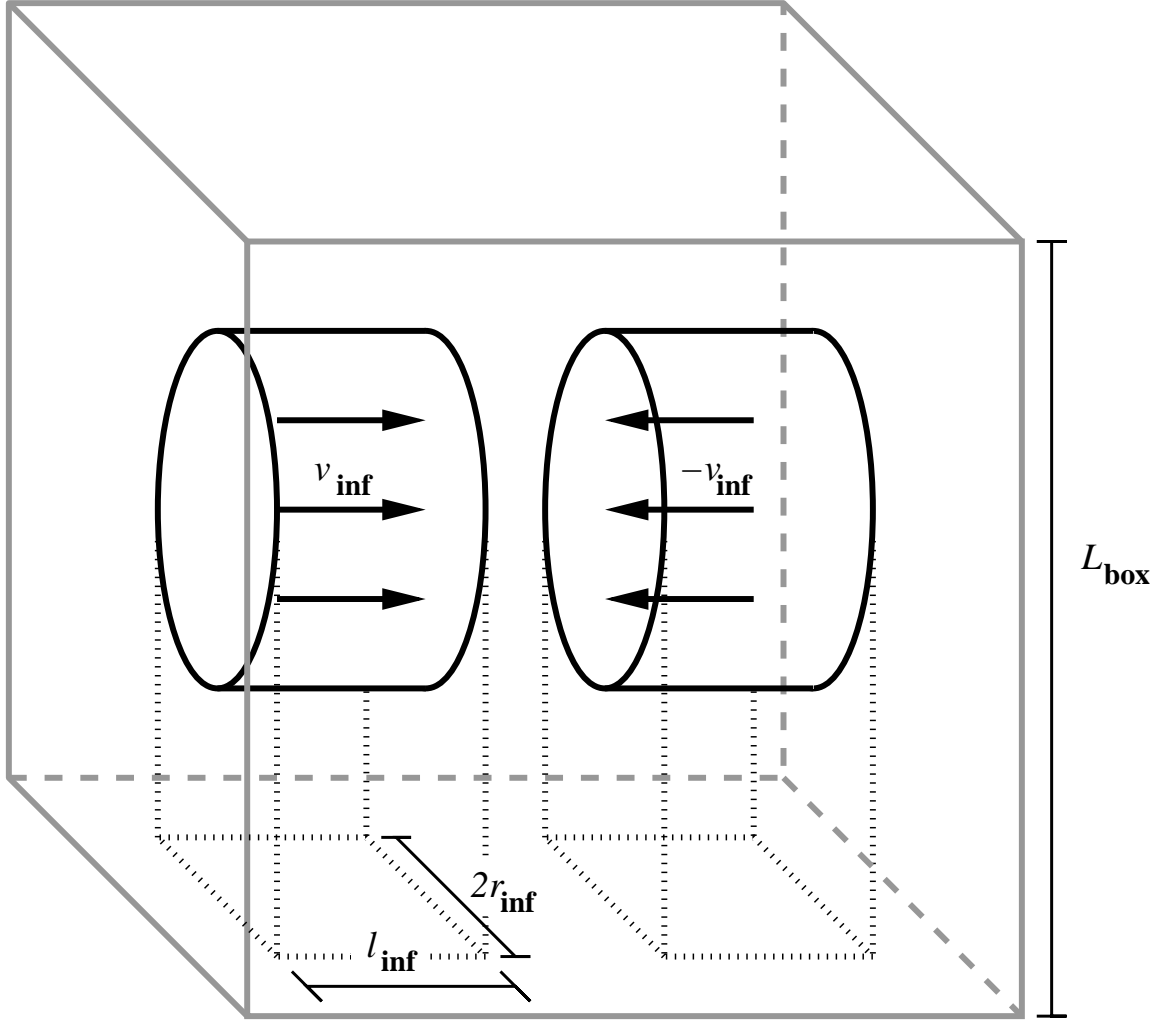


FIG. 1.— Setup of the simulations. Within a cubic box measuring L_{box} on a side, two cylindrical inflows, each of length ℓ_{inf} , radius r_{inf} , and aligned with the x -axis of the domain, are set to collide. The inflows have a velocity corresponding to $\mathcal{M}_{\text{inf}} = 1.22$ with respect to the undisturbed medium. Also, a fluctuating velocity field with amplitude $v_{\text{rms},i}$ is added at the beginning of the run in order to trigger the dynamical instability of the resulting compressed layer. Table 1 lists the values used for these parameters.

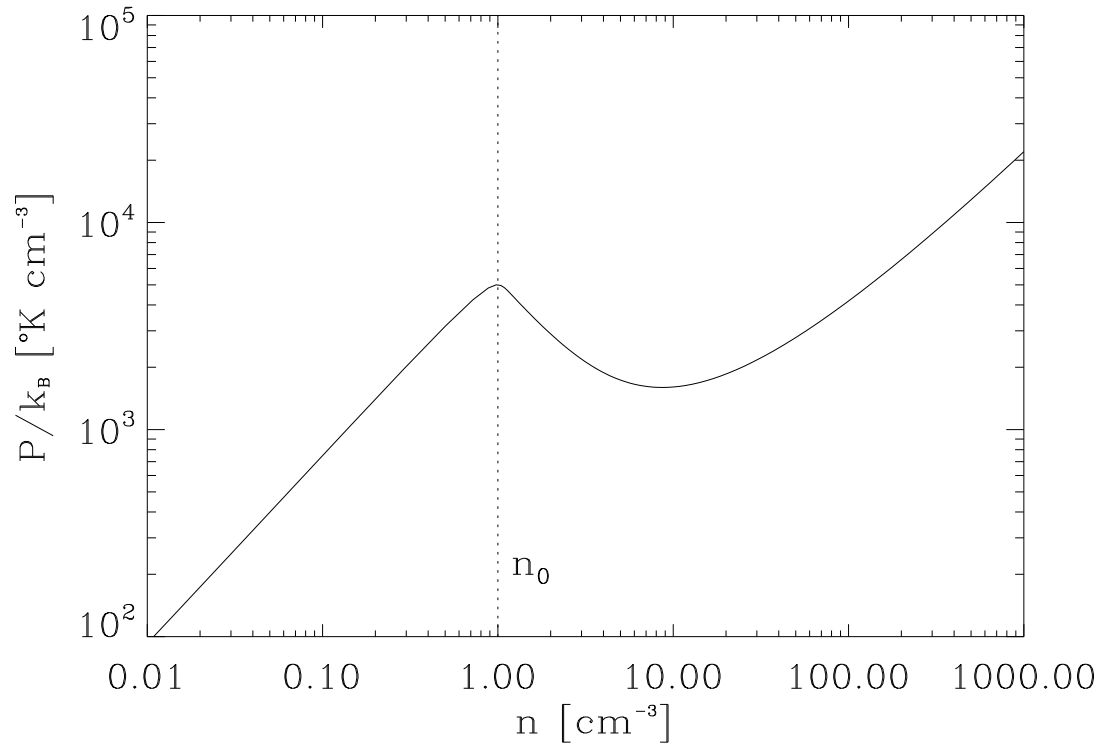


FIG. 2.— Thermal-equilibrium pressure *versus* density for the cooling and heating functions given by eqs. (3) and (4). The vertical *dotted* line indicates the uniform initial density in the simulations. The tangent to the curve at that location has a near-zero slope, indicating $\gamma_e \approx 0$. At $n = 0.2 \text{ cm}^{-3}$, $\gamma_e = 0.83$.

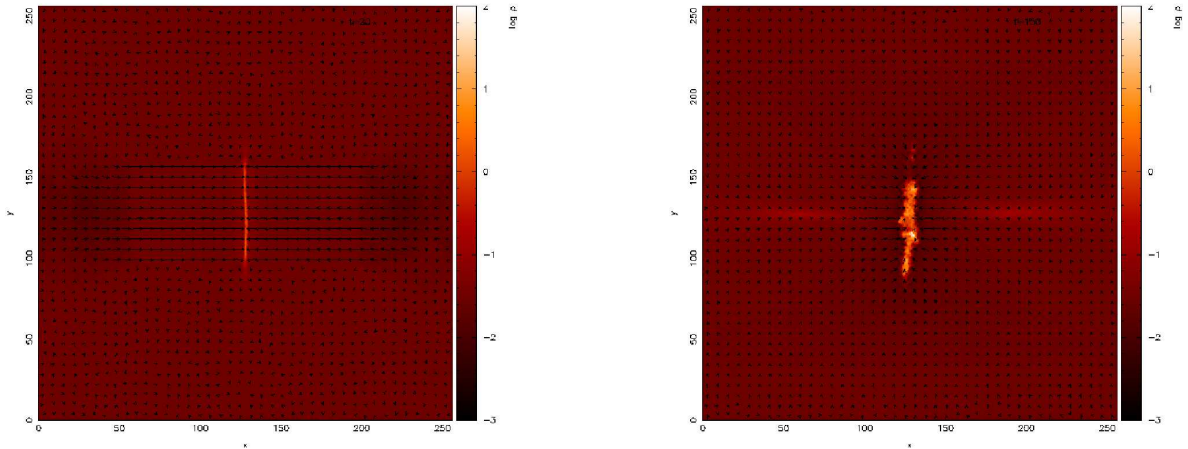


FIG. 3.— Edge-on views of run L256 Δv 0.17 at $t = 2.66 \text{ Myr}$ (*left*) and 20.0 Myr (*right*). The arrows indicate the velocity field. This figure is available as an mpeg animation in the electronic edition of *The Astrophysical Journal*.

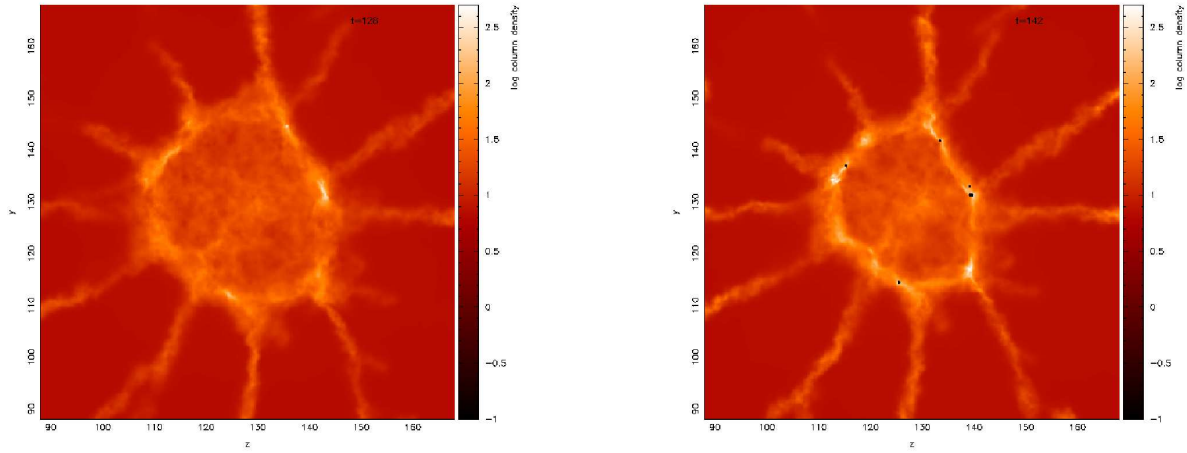


FIG. 4.— Face-on views of run L256 Δv 0.17 at $t = 17.0$ Myr (*left*) and 18.9 Myr (*right*). The dots indicate the projected positions of the sink particles. This figure is available as an mpeg animation in the electronic edition of *The Astrophysical Journal*.

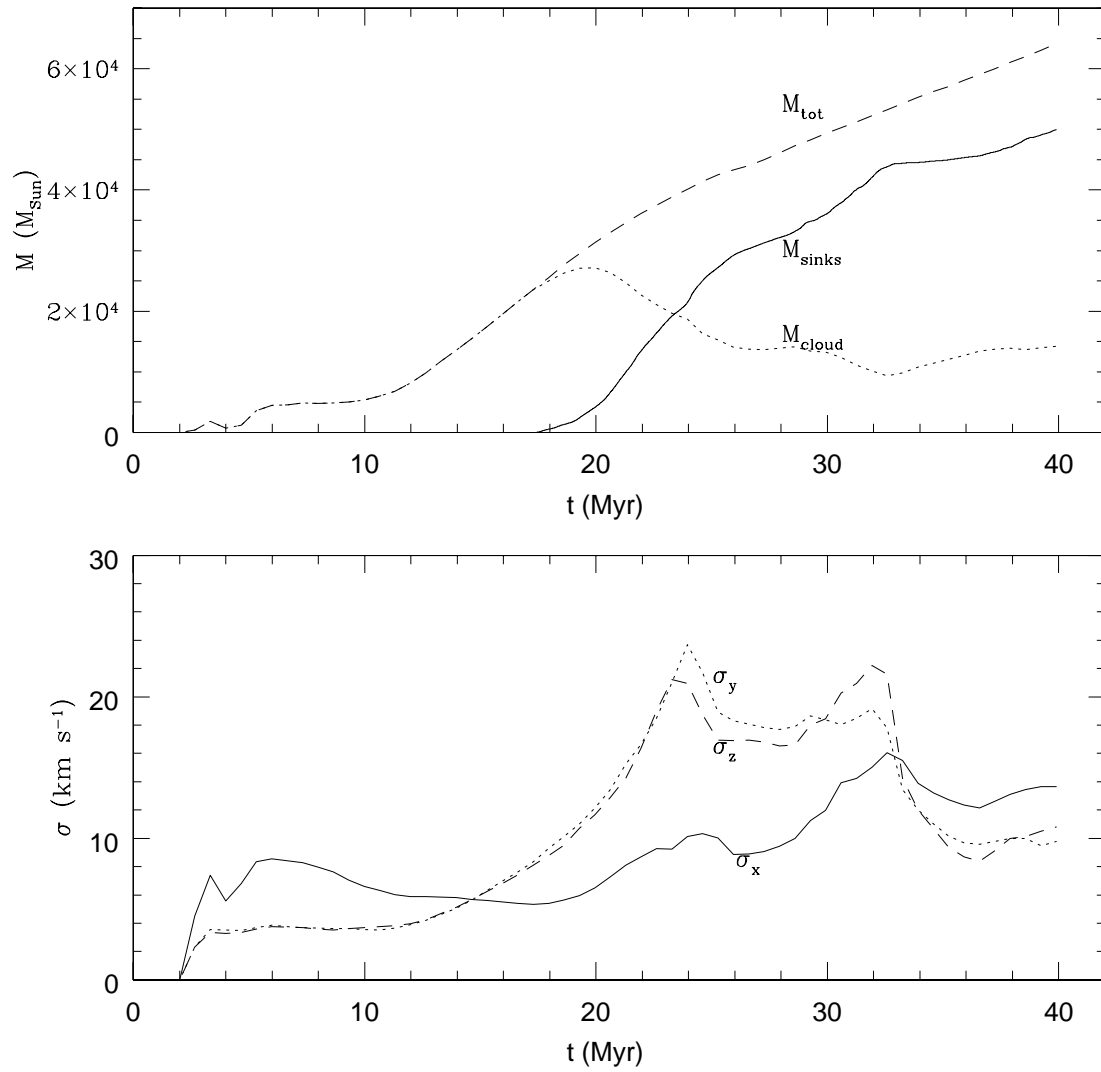


FIG. 5.— *Top*: Evolution of the cloud, sink, and total (cloud+sink) mass for run L256 Δv 0.17. *Bottom*: Evolution of the velocity dispersion of the dense gas ($n > 50 \text{ cm}^{-3}$) in each of the three coordinate axes. From $t \approx 6$ Myr through ≈ 12 Myr, σ_x decreases, reflecting the smooth end of the inflows. At this time, the gravitational collapse of the cloud (in the yz plane) sets in, generating an increase in σ_y and σ_z . While initially unaffected by this collapse, σ_x increases starting at $t \approx 18$ Myr, coinciding with the onset of star formation.

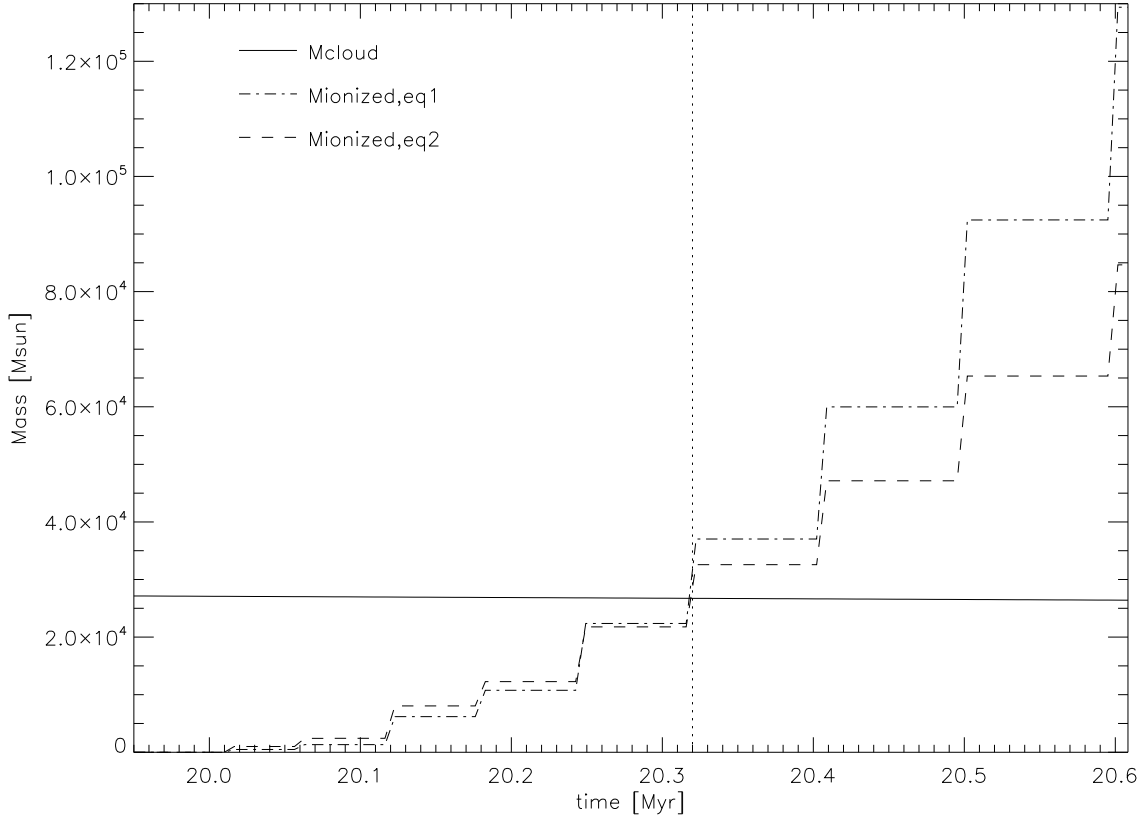


FIG. 6.— Evolution of the cloud mass and of the minimum mass that is not dispersed by stellar ionizing radiation under the two estimates given by eqs. (9) and (10) for run L256 Δv 0.17. The cloud is expected to be disrupted when the minimum cloud mass for non-disruption exceeds the actual cloud mass, at the time indicated by the vertical *dotted* line.

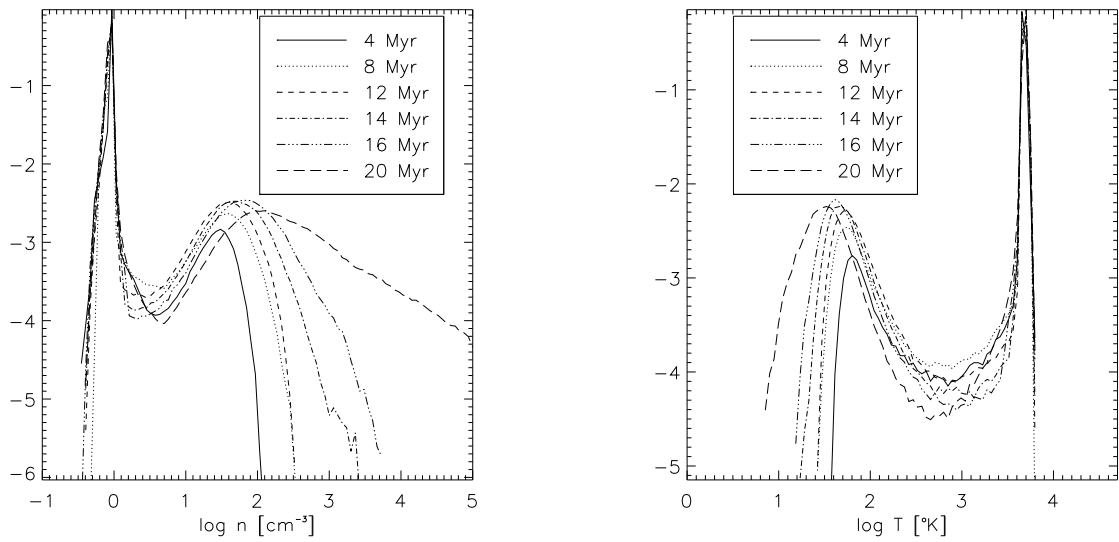


FIG. 7.— Evolution of the mass-weighted density (*left* frame) and temperature (*right* frame) histograms (normalized to the maximum) for run L256 Δv 0.17 at various times.

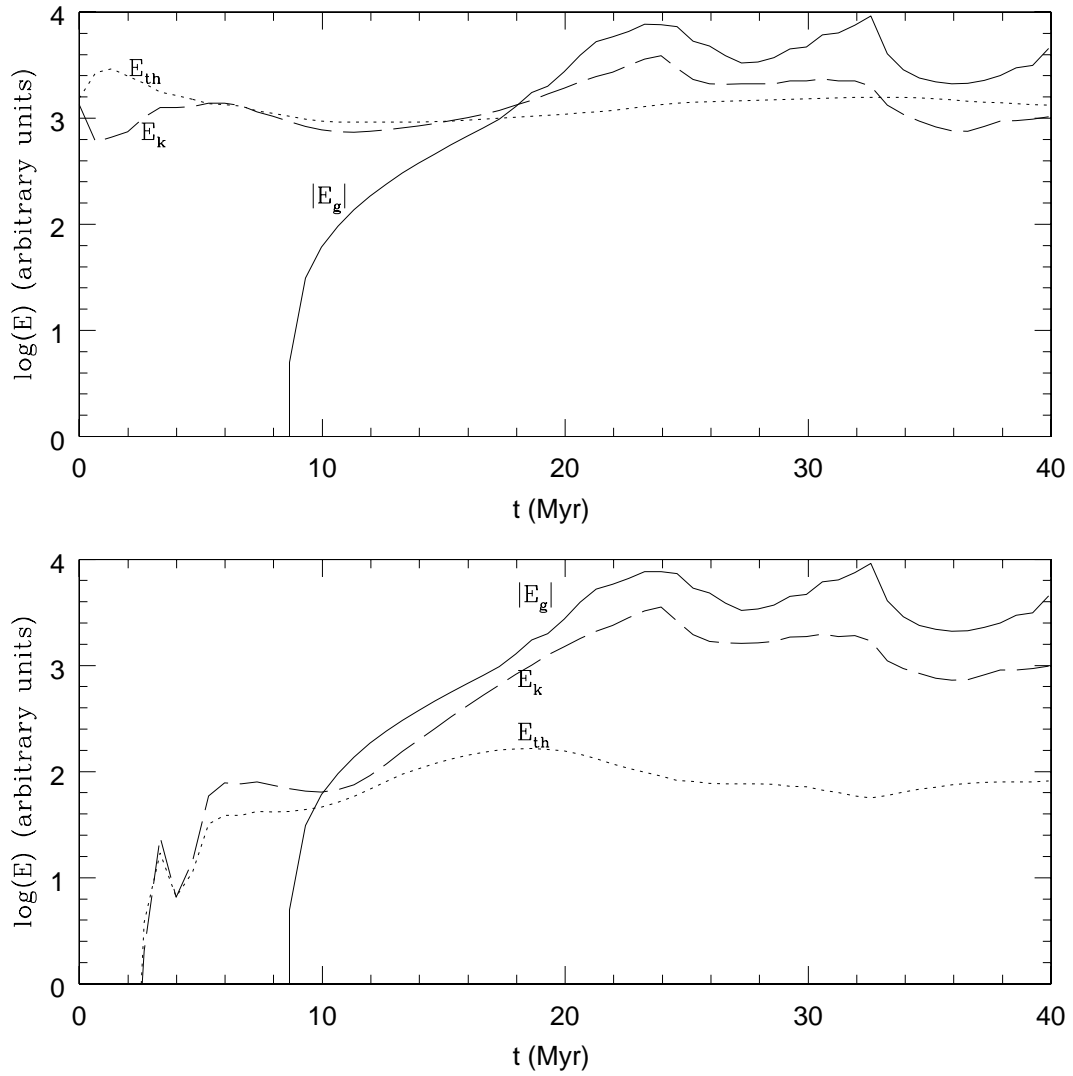


FIG. 8.— *Top*: Evolution of the total gravitational energy (in absolute value) of the numerical box and of the kinetic and thermal energies in a cylinder of radius 32 pc and length 16 pc centered in the middle of the numerical box for run L256 Δv 0.17. *Bottom*: Similar to the top panel, but with the thermal and kinetic energies calculated for the dense gas ($n > 50 \text{ cm}^{-3}$) only.

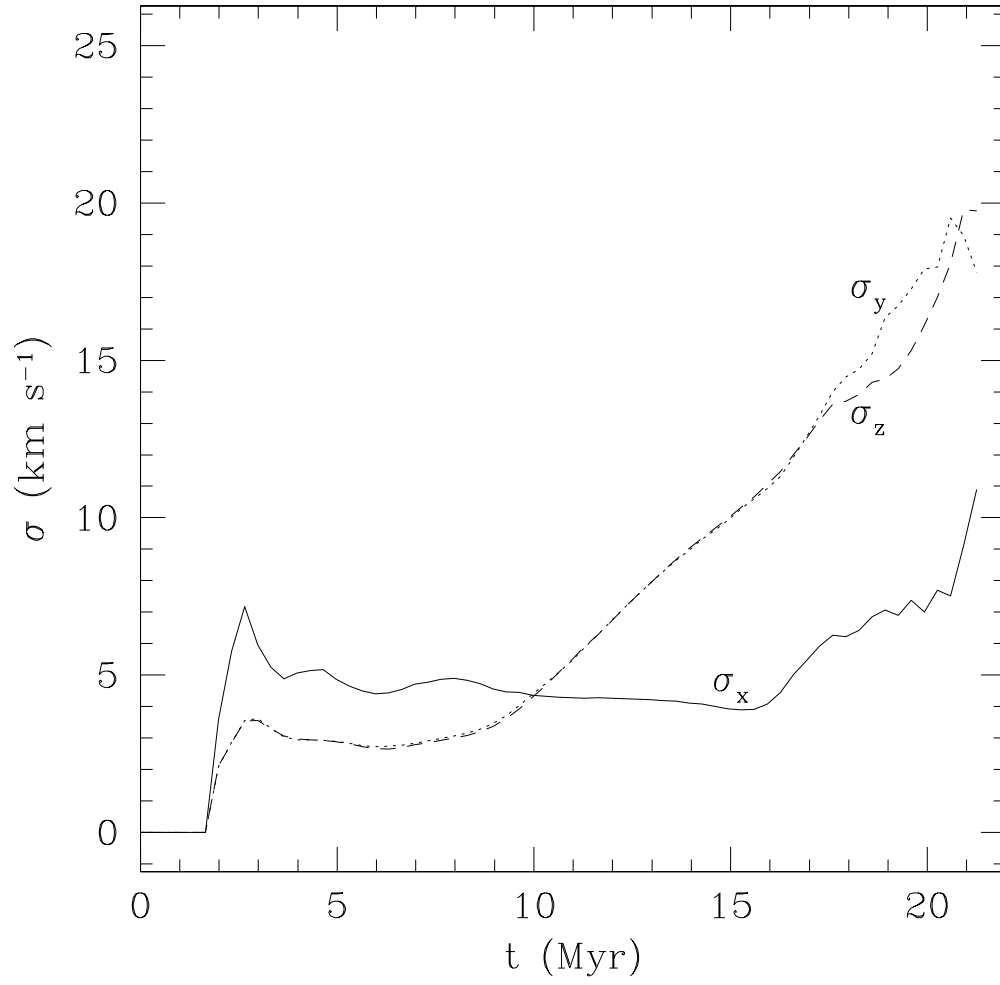


FIG. 9.— Evolution of the velocity dispersion in the dense gas ($n > 50 \text{ cm}^{-3}$) along each of the three coordinate axes for run L128 Δv 0.24. Compare to fig. 5 (*right*), noting the different extension of the axes.